Three thresholds and a computer-assisted phase diagram for the spectral stability of periodic hydroelastic Whitham waves

Lingsen Meng

Department of Earth, Planetary, and Space Sciences, University of California, Los Angeles, CA, USA

lsmeng@g.ucla.edu

Code, certificates and data: `https://doi.org/10.5281/zenodo.22973877`

Three thresholds and a computer-assisted phase diagram for the spectral stability of periodic hydroelastic Whitham waves

Lingsen Meng[a,*]

[a]*Department of Earth, Planetary, and Space Sciences, University of California, Los Angeles, Los Angeles, CA, USA*

Abstract

We study the spectral stability of 2π-periodic travelling waves of the hydroelastic Whitham equation, a scalar model with the full linear dispersion relation of water waves under a thin elastic sheet, as a function of the flexural rigidity T. Besides the modulational cluster at the origin, the zero-amplitude spectrum has, on an interval of T, a collision of opposite Krein signature between the carrier and the half-wavenumber mode, and three thresholds with closed forms in $\tanh \frac{1}{2}$, $\tanh 1$ and $\tanh 2$ organise the small-amplitude picture: modulational instability for $T_2 < T < T_0$ ($T_2 \approx 0.05585$, $T_0 \approx 0.16638$, the long-wave/short-wave resonance), sideband instability for $T_0 < T \leq T_1$ ($T_1 \approx 0.23108$), and spectral stability above T_1, so that the limiting stability threshold is T_1 and not the modulational threshold T_0. We prove this picture for all Bloch parameters, with explicit amplitude windows that shrink at the thresholds, by combining analytic reductions with remainder control and a computer-assisted proof in interval arithmetic at finite amplitude. For every amplitude $0 < a \leq 10^{-2}$ (height $H \lesssim 0.02$ of the depth) the waves are unstable for $T \in [0.0675, 0.16516] \cup [0.1681, T_1]$, and they are spectrally stable for $T \geq 0.231082819472$ with an amplitude window that closes linearly as $T \downarrow T_1$; a rescaling by $T^{-1/2}$ extends the small-amplitude stable statement uniformly to the purely flexural limit. Numerically, our computations reproduce those of Flamarion and Adriazola (2026), and the instabilities they report for $0.1 < T \leq 0.7$ at larger heights have their maximal growth at the Bloch band edge, consistent with a continuation of the sideband collision rather than a modulational instability.

Keywords: hydroelastic waves, Whitham equation, spectral stability, modulational instability, Krein collision, computer-assisted proof

1. Introduction

Periodic waves on the surface of a fluid covered by a thin elastic sheet (e.g. a floating ice cover or a very large floating structure) combine gravity with a restoring force from bending, which enters the linear dispersion relation through a term proportional to k^4. Whether such waves are stable, and what sets the boundary between stable and unstable regimes,

*Corresponding author.

Email address: `lsmeng@g.ucla.edu` (Lingsen Meng)

is a question that has been answered in a few asymptotic limits and otherwise mainly by numerical computation. In this paper we address it for the hydroelastic Whitham equation of Dinvay et al. [1], a scalar model that keeps the full linear dispersion relation of the problem under the sheet, and we give a phase diagram of the spectral stability of its 2π-periodic travelling waves in the flexural rigidity T that is proved, either analytically or by computer-assisted interval arithmetic, up to a wave height of $H \approx 0.02$ (in units of the depth), outside narrow windows at the thresholds where the admissible amplitude shrinks to zero.

The stability of these waves was studied numerically by Flamarion and Adriazola [2], who computed the Bloch spectra of waves with heights between 0.05 and 0.5 by the Fourier–Floquet–Hill method and reported a sequence of regimes in T. For weak elasticity the classical figure-eight instability appears, at $T = 0.1$ even small waves are unstable, at $T = 0.45$ small waves are stable and lose stability as the height grows, and for $T > 0.7$ all waves they computed are stable. Their study is numerical and makes no claim of rigour, and the location of the boundary between the small-amplitude instability at $T = 0.1$ and the small-amplitude stability at $T = 0.45$ is not resolved there, and neither is the mechanism that destabilises the waves at $T = 0.45$. On the rigorous side, Hsiao et al. [3, 4] recently resolved the four Bloch eigenvalues near the origin for small hydroelastic Stokes waves of the full Euler equations, in finite and in infinite depth, and obtained an explicit Benjamin–Feir index in the depth, the surface tension and the bending coefficient. Their analysis is restricted to Bloch parameters near zero and excludes a resonance set and a characteristic-collision set, so that it describes the modulational part of the spectrum but not the rest of it.

For small waves the long-wave part of the spectrum is governed by a modulational instability index. Hur and Johnson [5, 6] derived such an index for Whitham-type equations with a general symbol and listed the mechanisms through which it can change sign, one of which is the resonance between the group velocity of the carrier and the phase velocity of the longest waves. Evaluated on the hydroelastic symbol, this resonance occurs at a single rigidity $T_0 \approx 0.16638$, and small waves are modulationally unstable for $T_2 < T < T_0$, where T_2 is introduced below. We make no claim of novelty for this identification. However, the modulational index describes only the eigenvalues near the origin, and our first observation is that it does not decide stability here. For T between T_0 and a second threshold $T_1 \approx 0.23108$, at which the half-wavenumber mode travels with the phase speed of the carrier ($m_T(1/2) = m_T(1)$), the zero-amplitude spectrum has a pair of collisions of opposite Krein signature at Bloch parameters of order one, and these collisions open an instability whose growth rate is of order a, larger than the modulational rate of order a^2. Thus the limiting small-amplitude stability threshold is T_1 and not T_0 (our stability theorem starts at $T_1 + 3.9 \times 10^{-6}$, and the amplitude window closes as $T \downarrow T_1$). A third threshold, $T_2 \approx 0.05585$, where the group-velocity dispersion of the carrier vanishes, bounds from below the range in which the sign of the modulational index is the sign of $R(T) = \Psi'(1) - 1$. All three thresholds have closed forms in $\tanh \frac{1}{2}$, $\tanh 1$ and $\tanh 2$ (Proposition 2).

Our main results make this picture rigorous with explicit amplitude windows, in two layers. The first layer consists of analytic reductions with remainder control, evaluated in interval arithmetic: a two-mode Feshbach reduction for the sideband collision, a three-mode reduction and the exact closed form $\alpha_6 = 2WR^3(2D - R)/D$, $\alpha_8 = W^2R^4$ of the leading coefficients of the modulational discriminant, and, on the stable side, disc-counting arguments that use the symmetry $\lambda \mapsto -\bar{\lambda}$ of the spectrum. These give instability on

$[0.06, T_0 - 10^{-6}]$ and on $[T_0 + 1.3 \times 10^{-8}, T_1]$, and spectral stability for every Bloch parameter for $T \geq T_1 + 3.9 \times 10^{-6}$, at amplitudes of $\sim 10^{-6}$ to $\sim 10^{-3}$ depending on the segment (Theorem 4). The second layer is a computer-assisted proof at finite amplitude, in which the travelling wave, the truncated Bloch matrix and its tail are enclosed on boxes in the parameters (T, a) and the relevant eigenvalues are either enclosed off the imaginary axis (for instability) or counted and pinned to it (for stability). Together the two layers give, for every $0 < a \leq 10^{-2}$, modulational instability on $T \in [0.0675, 0.16516]$, sideband instability on $T \in [0.1681, T_1]$, and spectral stability for all Bloch parameters on $T \geq 0.231082819472$ with an amplitude window $a^*(T) \geq \min(10^{-2}, (T - T_1)/4.235)$ (Theorem 5). The windows shrink at the two thresholds, as they must, since the governing indices vanish there. For large rigidity we rescale by $\delta = T^{-1/2}$ and prove the stable statement uniformly in $\delta \in [0, 10^{-1/2}]$, including the purely flexural limit $\delta = 0$ (Theorem 6).

The same numerical code that we use to choose parameters for the proofs reproduces the computations of Flamarion and Adriazola, and it adds one observation to their picture (Section 9): for $T \geq 0.1$ and heights $H \geq 0.1$ the most unstable eigenvalue sits at the band edge $\xi = 1/2$, which is consistent with the instability they observe at $T = 0.45$ for $H \gtrsim 0.2$ being a continuation of the sideband collision born at T_1, rather than a modulational instability; we have not tracked the eigenpair continuously to confirm the identification. Its onset height increases with T and passes $H = 0.5$ near $T \approx 0.76$, which is consistent with the cut-off near $T = 0.7$ in their computations. This observation is numerical, although it is supported by a close agreement with their growth rates, and our proofs cover only heights $H \lesssim 0.02$.

Computer-assisted proofs have entered the study of Whitham-type equations only recently. Cadiot [7] proved the existence and spectral stability of solitary waves of the Whitham and capillary-gravity Whitham equations by a Newton–Kantorovich argument in weighted Fourier spaces. Our setting differs in that the waves are periodic, so that stability has to be controlled for a continuum of Bloch parameters, the operators are not self-adjoint, and the symbol grows like $|k|^{3/2}$. Moreover, on the unstable side the proof has to enclose an eigenvalue off the imaginary axis, whereas on the stable side it has to account for every eigenvalue. Computer-assisted Floquet and spectral methods have a longer history for other problems, e.g. rigorous Floquet theory for periodic orbits [8], spectral stability for a periodically forced wave equation [9] and periodic travelling waves with a nonlocal reaction term [10]. We are not aware of an earlier computer-assisted proof of spectral stability for all Bloch parameters of periodic travelling waves of a nonlocal dispersive equation.

The paper is organised as follows. Section 2 fixes the setting and the Bloch problem, and Section 3 classifies the zero-amplitude collisions and derives the three thresholds. Section 4 states the main theorems. Sections 5 and 6 give the small-amplitude layer for the unstable and the stable segments, respectively, Section 7 the computer-assisted layer, and Section 8 the large-rigidity limit. Section 9 compares our results with numerical computations, including those of Flamarion and Adriazola, and Section 10 discusses the relation to the Euler problem and the limitations of our results. All proofs were produced and checked by one project, with the help of AI agents, and no party independent of it has re-derived them (Section 10 and Appendix Appendix B describe what independence the checks do provide).

2. Setting

2.1. The equation and its travelling waves

We consider the hydroelastic Whitham equation of Dinvay et al. [1],

$$
\begin{aligned}
&u_t + 2uu_x + K_T u_x = 0, \qquad \widehat{K_T g}(k) = m_T(k)\,\hat{g}(k),\\
&m_T(k) = \sqrt{(1+Tk^4)\,\frac{\tanh k}{k}}, \quad m_T(0) = 1,
\end{aligned}
\tag{1}
$$

in which the fluid depth, the gravitational acceleration and the density have been scaled to one and $T > 0$ is the dimensionless flexural rigidity of the elastic sheet (the term Tk^4 replaces the capillary term Tk^2 of the capillary-gravity Whitham equation). For large $|k|$ the symbol grows like $\sqrt{T}\,|k|^{3/2}$, so that K_T is a nonlocal operator of order 3/2, and all tail estimates below are built on explicit lower bounds of this growth rather than on its asymptotic form.

A travelling wave $u(x,t) = f(x-ct)$ with period 2π satisfies, after one integration,

$$
-cf + f^2 + K_T f = b. \tag{2}
$$

We work with even, zero-mean solutions normalised by the first Fourier coefficient, $\hat{f}_1 = \hat{f}_{-1} = a/2$, so that $f = a\cos z + O(a^2)$ and the height $H = f(0) - f(\pi) = 2a + O(a^3)$ (for example, $a = 10^{-2}$ gives $H = 0.0200$). The zero-mean condition forces $b = \langle f^2 \rangle$, and b cannot be set to zero at the same time. Several numerical studies, including Sanford et al. [11] and Flamarion and Adriazola [2], use the other normalisation $b = 0$. The two are equivalent, and we state the equivalence here because every comparison with those studies in Section 9 depends on it.

Lemma 1 (Galilean gauge)**.** *Let (f, c, b) solve (2) and let $\gamma \in \mathbb{R}$. Then $g = f + \gamma$ and $c' = c + 2\gamma$ solve $-c'g + g^2 + K_T g = b - c\gamma - \gamma^2 + \gamma$, and $c' - 2g = c - 2f$ pointwise. In particular, for $c \neq 1$ the choice $\gamma = 2b/\big((c-1) + \operatorname{sign}(c-1)\sqrt{(c-1)^2 + 4b}\big)$, the root of $\gamma^2 + (c-1)\gamma - b = 0$ that vanishes with b, gives the $b = 0$ normalisation, and the two waves have the same height and the same Bloch operators* (3)*.*

Proof. Since $m_T(0) = 1$, K_T maps constants to themselves, and the first identity follows by expanding $-(c+2\gamma)(f+\gamma) + (f+\gamma)^2 + K_T f + \gamma$. The second is immediate, and the operators (3) depend on the wave only through $c - 2f$. Since $b = \langle f^2 \rangle \geq 0$, the square root is real. □

The identity was also checked in exact arithmetic, and on a computed wave at $T = 0.45$, $a = 0.02$ the shifted wave solves the $b = 0$ equation to a residual of $\sim 4 \times 10^{-17}$ with an unchanged height (`paper/checks/check_gauge.py`). Since $c \to m_T(1)$ as $a \to 0$, and $m_T(1) < 1$ exactly for $T < 1/\tanh 1 - 1 \approx 0.3130$, the small root is the one with the minus sign there and the one with the plus sign for larger T; either way it selects the $b = 0$ branch that bifurcates from $u = 0$. The other root gives a gauge-equivalent wave with the same spectrum.

2.2. Bloch operators and spectral stability

Linearising (1) about f in the moving frame $z = x - ct$ and applying the Bloch transform with parameter $\xi \in [-1/2, 1/2]$ gives the family of operators on $L^2(\mathbb{T})$

$$\mathcal{L}_\xi v = (\partial_z + i\xi)\big((c-2f)v - K_{T,\xi}v\big), \qquad \widehat{K_{T,\xi}v}(n) = m_T(n+\xi)\,\hat{v}(n). \tag{3}$$

In Fourier variables $\mathcal{L}_\xi = iM(\xi)$ with $M = DA$, where $D = \operatorname{diag}(n+\xi)$ and $A_{nm} = (c - m_T(n+\xi))\delta_{nm} - 2\hat{f}_{n-m}$. For an even real wave both D and A are real, and A is symmetric. Therefore $M(\xi)$ is a real operator, its spectrum is symmetric under complex conjugation, and the spectrum of $\mathcal{L}_\xi$ is symmetric under $\lambda \mapsto -\bar{\lambda}$. In addition, reflection $z \mapsto -z$ gives $M(-\xi) = -PM(\xi)P$ with P the index reversal, so that it suffices to consider $\xi \in [0, 1/2]$. The symmetry under $\lambda \mapsto -\bar{\lambda}$ is the mechanism behind every stability argument in this paper: an eigenvalue of $\mathcal{L}_\xi$ that can be isolated in a disc centred on the imaginary axis, with no other eigenvalue in that disc, is its own mirror image and is therefore purely imaginary.

We say that the wave is *spectrally stable* if $\sigma(\mathcal{L}_\xi) \subset i\mathbb{R}$ for every $\xi \in [-1/2, 1/2]$, and *spectrally unstable* if some $\mathcal{L}_\xi$ has an eigenvalue with $\operatorname{Re}\lambda > 0$. By the Bloch decomposition the second statement places λ in the spectrum of the linearisation on $L^2(\mathbb{R})$ (as a point of the continuous spectrum, since a Bloch eigenfunction is not square integrable on the line). We make no claim about nonlinear or orbital stability.

2.3. Zero amplitude

At $a = 0$ the operator $\mathcal{L}_\xi$ is diagonal, with eigenvalues $i\Omega_n(\xi)$,

$$\Omega_n(\xi) = \varphi_T(n+\xi), \qquad \varphi_T(k) = k\left(m_T(1) - m_T(k)\right). \tag{4}$$

Since the symbol is even, φ_T is odd and vanishes at $k = 0, \pm 1$. For $a \neq 0$ small, the symmetry above implies that a simple eigenvalue stays on the imaginary axis, so that instability can only be born where two or more of the curves (4) meet. The next section classifies these meetings, and it is there that the three thresholds of this paper appear.

3. Collisions at zero amplitude and three thresholds

A collision of the curves (4) is a solution of $\varphi_T(x) = \varphi_T(x+j)$ with $x = n + \xi$ and $j \geq 1$ an integer. Every $\xi = 0$ carries the triple collision of the modes $n = -1, 0, 1$ (all three eigenvalues vanish), which is the origin of the modulational problem. Our first observation is that, at least for $T > 0.1263$, only one further type of collision can occur apart from this triple point, and that whether it occurs is decided by the signs of two elementary functions of T.

3.1. The indices

Define

$$R(T) = m_T(1) - m_T(0) + m_T'(1) = \Psi'(1) - m_T(0), \tag{5}$$
$$S(T) = m_T(1) - m_T(1/2), \tag{6}$$
$$W(T) = \Psi''(1), \qquad D(T) = m_T(2) - m_T(1), \tag{7}$$

where $\Psi(k) = k\, m_T(k)$ is the dispersion relation, so that $\Psi'(1)$ is the group velocity of the carrier and W its group-velocity dispersion. R compares the group velocity of the carrier with the phase velocity $m_T(0) = 1$ of the longest waves, S compares the phase velocity of the carrier with that of the half-wavenumber mode (the mode that sits at the edge $\xi = 1/2$ of the Brillouin zone), and D measures the distance from the 1:2 (Wilton-type) resonance of the carrier with its second harmonic. All four are explicit in T, $\tanh\frac{1}{2}$, $\tanh 1$ and $\tanh 2$, and so are their zeros.

Proposition 2 (three thresholds)**.** *Let $t_{1/2} = \tanh\frac{1}{2}$, $t_1 = \tanh 1$, $t_2 = \tanh 2$, $s_1 = \operatorname{sech}^2 1$ and $A = (5t_1 + s_1)/(2\sqrt{t_1})$, $B = 2\sqrt{t_1}$. On $T > 0$:*

1. *$R(T) = A\sqrt{1+T} - B/\sqrt{1+T} - 1$ is strictly increasing and has exactly one zero,*
$$T_0 = \Big(\frac{1+\sqrt{1+4AB}}{2A}\Big)^2 - 1 = 0.16637\,65066\,72063\ldots;$$
2. *$S(T) = 0$ is equivalent to the linear equation $t_1(1+T) = 2t_{1/2}(1+T/16)$, so that S has exactly one zero,*
$$T_1 = \frac{2t_{1/2} - t_1}{t_1 - t_{1/2}/8} = 0.23107\,89132\,21830\ldots,$$
and $S > 0$ if and only if $T > T_1$;
3. *$W(T) = N(T)/(4m_T(1)^3)$, where $N = 2hh'' - (h')^2 + 4hh'$ evaluated at $k = 1$, with $h(k) = (1 + Tk^4)\tanh k/k$, and*
$$N(T) = c_2T^2 + c_1T + c_0, \quad c_2 = 15t_1^2 + 10s_1t_1 - s_1^2 - 4s_1t_1^2,$$
$$c_1 = 2(15t_1^2 + 6s_1t_1 - s_1^2 - 4s_1t_1^2), \quad c_0 = -\big((t_1 - s_1)^2 + 4s_1t_1^2\big).$$
Since $c_2 > 0 > c_0$, N has one negative and one positive zero, and $T_2 = \big(-c_1 + \sqrt{c_1^2 - 4c_2c_0}\big)/(2c_2) = 0.05584\,53094\,24050\ldots$ is the only zero on $T > 0$; $W > 0$ exactly for $T > T_2$;
4. *$D(T) = 0$ exactly at $T_D = (t_1 - t_2/2)/(8t_2 - t_1) = 0.04022\,37649\ldots$, and $D > 0$ for $T > T_D$.*

Proof. With h as in (3), $m_T = \sqrt{h}$ and $2m_Tm_T' = h'$. At $k = 1$ one has $h = (1+T)t_1$ and $h' = 4Tt_1 + (1+T)(s_1 - t_1)$, and substituting gives the stated form of R with $u = 1+T$. Both A and B are positive, so R is strictly increasing in u, tends to $-\infty$ as $u \to 0^+$ and to $+\infty$ as $u \to \infty$, and the zero solves $Au - \sqrt{u} - B = 0$ as a quadratic in $\sqrt{u}$. Items 2 and 4 follow by squaring $m_T(1) = m_T(1/2)$ and $m_T(2) = m_T(1)$, both sides being positive, and noting $t_1 > t_{1/2}/8$ and $8t_2 > t_1$. For item 3, $\Psi'' = m_T'' + 2m_T'$ and $m_T'' = h''/(2m_T) - (h')^2/(4m_T^3)$; at $k = 1$ one has $h = (1+T)t_1$, $h' = 4Tt_1 + (1+T)(s_1 - t_1)$ and $h'' = 12Tt_1 + 8T(s_1 - t_1) + 2(1+T)(t_1 - s_1 - s_1t_1)$, all affine in T, and expanding gives the coefficients above. For the signs, $0 < s_1 < t_1 < 1$ gives $s_1^2 < s_1t_1$ and $4s_1t_1^2 < 4s_1t_1$, hence $c_2 > 15t_1^2 + 5s_1t_1 > 0$, while $c_0 < 0$ is evident. □

All identities and the four numbers were checked in exact symbolic arithmetic and agree with the values used elsewhere in this paper to at least 17 digits (`paper/checks/`

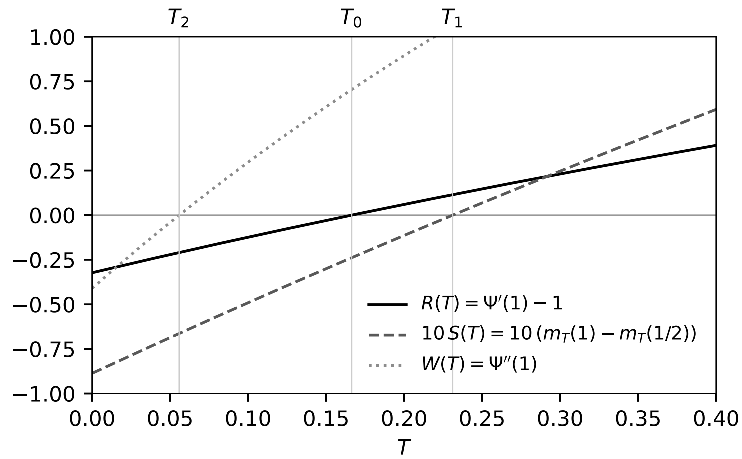

Figure 1: The indices R, S (scaled by 10) and W against T, with their zeros T_0, T_1 and T_2.

`check_thresholds.py`). It is worth noting that $T_2 < T_0 < T_1$, and that on $T > T_2$ the three quantities W, D and $2D - R$ are positive ($W > 0$ by item 3, $D > 0$ by item 4 since $T_2 > T_D$, and $2D - R > 0.32$ on all of $T > T_2$, certified in Arb ball arithmetic on $[T_2, 100]$ and by the elementary bounds $m_T(2) \geq 4\sqrt{T}\sqrt{t_2/2}$, $m_T(1) \leq \sqrt{(1+T)t_1}$ and $m_T'(1) \leq 2\sqrt{t_1 T}$ for $T \geq 100$; `paper/checks/check_2DmR_arb.py`), which is what makes the sign of the modulational index equal to the sign of R in Section 5.

3.2. Which collisions can occur

Write $g(x) = \varphi_T(x) - \varphi_T(x+1)$. A direct computation gives

$$g(0) = g(-1) = 0, \qquad g(-1-x) = g(x), \qquad g'(0) = R(T), \qquad g(-\tfrac{1}{2}) = -S(T). \tag{8}$$

In addition, where φ_T is strictly monotone on $|k| \geq 1$ collisions with $j \geq 3$ are excluded and the only $j = 2$ collision is the trivial one at $x = -1$ (the triple point at $\xi = 0$). This monotonicity needs $\varphi_T'(1) = -m_T'(1) < 0$, which holds only for $T > (t_1 - s_1)/(3t_1 + s_1) \approx 0.1263$, and for smaller T the curve φ_T first rises beyond $k = 1$, and we do not attempt a classification there. On $T > 0.1263$ we have checked the monotonicity and the restriction to $j \leq 2$ on a grid of T values. In that range, therefore, every nontrivial collision is a $j = 1$ collision between the modes n and $n + 1$ at a zero of g in $(-1, 0)$. By (8), g leaves the two ends of this interval towards the negative side when $R > 0$ and takes the value $-S$ at the midpoint, so that for $R > 0 > S$ there is a symmetric pair of zeros $x_* \in (-1, -\frac{1}{2})$ and $-1 - x_*$. This is the case exactly for $T_0 < T < T_1$.

At such a collision the 2×2 block of $\mathcal{L}_\xi$ on the modes $n, n+1$ has off-diagonal product $(-iax_*)(-ia(x_*+1)) = -a^2 x_*(x_*+1) > 0$ to leading order, so that the colliding eigenvalues split as $i\Omega \pm |a|\sqrt{-x_*(x_*+1)} + O(a^2)$. The collision has opposite Krein signatures, and it opens a bubble of instability with growth rate $\sim |a|\kappa$, $\kappa = \sqrt{-x_*(x_*+1)} \leq 1/2$, the maximum $1/2$ being reached at the band edge. We call this the *sideband* instability. It is of order a, whereas the modulational instability near $\xi = 0$ is of order a^2, and it survives up to T_1 itself, where $x_* = -1/2$ and $\kappa = 1/2$.

The statement "no zero of g in $(-1,0)$ when $R<0$ or $S>0$" uses the shape of g and not only (8). It has been verified on a grid of T values, and it is implied rigorously on the stable segment by the stability theorems of Section 6 (which bound the zero-amplitude gaps from below on every T box they cover). However, a uniform proof for all T outside the stable segment is not part of this paper, and nothing below depends on it: the instability theorems of Sections 5 and 7 construct the unstable eigenvalue directly.

The resulting picture at small amplitude, which the rest of the paper makes rigorous with explicit amplitude windows, has three segments separated by T_0 and T_1:

- for $T_2 < T < T_0$ ($R<0$) the triple point at $\xi = 0$ opens into a modulational band (segment A);
- for $T_0 < T \le T_1$ the modulational band is closed ($R>0$), but a sideband collision exists and is unstable (segment B);
- for $T > T_1$ ($R>0$, $S>0$) neither mechanism is present, and the waves are spectrally stable (segment C; proved from $T_1 + 3.9\times10^{-6}$ on).

The first threshold, T_0, is the long-wave/short-wave resonance of Hur and Johnson [6], mechanism (2) in their list, evaluated on the flexural symbol, and we make no claim of novelty for its location. The second, T_1, and the sideband segment it closes, do not appear in the modulational analysis at all, because they live at $\xi = O(1)$, and in particular the limiting small-amplitude stability threshold is T_1 and not T_0. The theorems of the following sections prove this picture on closed T intervals that approach, but do not reach, T_0 and T_1 (Theorem 4).

4. Main results

Throughout, a is the amplitude parameter of Section 2 ($\hat{f}_1 = a/2$, $H = 2a + O(a^3)$), and "for all ξ" means every $\xi \in [-1/2, 1/2]$ and every eigenvalue of $\mathcal{L}_\xi$. The words *computer-assisted* mean that the statement rests on interval-arithmetic computations whose code, inputs and outputs are archived with their sha256 hashes and can be re-run (Appendix Appendix B).

Theorem 3 (modulational discriminant)**.** *For $T > T_D$ and (a,ξ) small, the three eigenvalues of $M(\xi)$ that bifurcate from the triple zero at $a=\xi=0$ are the roots of a real cubic whose discriminant has the form $\xi^6\,\Phi(a,\xi)$, with Φ analytic, even in a and in ξ, and*

$$\Phi(a,\xi) = \alpha_6 a^2 + \alpha_8 \xi^2 + O\big((a^2+\xi^2)^2\big), \qquad \alpha_6 = \frac{2WR^3(2D-R)}{D}, \qquad \alpha_8 = W^2R^4.$$

In particular $\alpha_6 = R^2\,\Delta_{\mathrm{MI}}$, where $\Delta_{\mathrm{MI}} = -2WR(R-2D)/D$ is the Hur–Johnson index [6] evaluated on m_T, and on $T > T_2$ one has $\operatorname{sign}\alpha_6 = \operatorname{sign} R$.

Theorem 4 (small amplitude; computer-assisted)**.** *(A) For every $T \in [0.06, T_0 - 10^{-6}]$ there is $a_A(T) > 0$ such that for $0 < a \le a_A(T)$ the operator $\mathcal{L}_{\tau a}$ has an eigenvalue with* $\operatorname{Re}\lambda \ge c(T)\,a^2 > 0$ *for a suitable $\tau = \tau(T)$. One may take $a_A = 1.06\times10^{-6}$ on* $[0.06, 0.09]$*, 3.56×10^{-6} on* $[0.09, 0.13]$*, 7.0×10^{-7} on* $[0.13, 0.15]$ *and* 1.65×10^{-7} *on* $[0.15, 0.16]$*; closer to T_0 the admissible a_A decreases like $(T_0 - T)^{3/2}$.*

(B) *For every* $T \in [T_0 + 1.30 \times 10^{-8}, T_1]$ *there is* $a_B(T) > 0$ *such that for* $0 < a \leq a_B(T)$ *the operator* $\mathcal{L}_{\xi_*(T)}$*, at the sideband collision point* $\xi_*(T)$*, has an eigenvalue with* $\operatorname{Re}\lambda \geq |a|\kappa(T)/2$*,* $\kappa = \sqrt{-x_*(x_* + 1)}$*. One may take* $a_B = 10^{-3}$ *on* $[0.22, T_1]$ *and* 1.99×10^{-4} *on* $[0.18, 0.22]$*; closer to* T_0 *the admissible* a_B *decreases like* $(T - T_0)^2$*.*

(C) *For every* $T \geq T_1 + 3.9 \times 10^{-6}$ *there is* $a_C(T) > 0$ *such that for* $0 < a \leq a_C(T)$ *the wave is spectrally stable. One may take* $a_C = 5 \times 10^{-5}$ *on* $[0.24, 10]$*, and* $a_C(T) \approx 0.01\,(T - T_1)$ *as* $T \downarrow T_1$*.*

Theorem 5 (finite amplitude; computer-assisted)**.** *Let* $0 < a \leq 10^{-2}$*.*

(A) *For* $T \in [0.0675, 0.16516]$ *the wave is spectrally unstable.*

(B) *For* $T \in [0.1681, T_1]$ *the wave is spectrally unstable.*

(C) *For* $T \geq 0.231082819472$ *and* $a \leq a^*(T)$*, where* $a^*(T) \geq \min\bigl(10^{-2}, (T - T_1)/4.235\bigr)$*, the wave is spectrally stable. In particular* $a^* = 10^{-2}$ *for* $T \geq T_1 + 0.04235 = 0.27343\ldots$*.*

On the two unstable segments the eigenvalue in (A) sits on the fibre $\xi = \tau a$ inside the modulational band, and the one in (B) at the sideband collision $\xi_*(T)$; in both cases the proof gives a positive lower bound for $\operatorname{Re}\lambda$ on every parameter box. On the stable segment the statement covers every Bloch parameter and every eigenvalue, including the high-frequency part of the spectrum.

Theorem 6 (large rigidity and the flexural limit; computer-assisted)**.** *Let* $\delta = T^{-1/2}$ *and* $\tilde{a} = a\delta$*. For every* $\delta \in [0, 0.3163]$*, every* ξ *and every* $0 < |\tilde{a}| \leq 4.6 \times 10^{-4}$*, the rescaled Bloch operators (Section 8) have purely imaginary spectrum. Consequently every wave with* $T \geq 473$ *and* $0 < a \leq 10^{-2}$ *is spectrally stable. For* $\delta = 0$ *the statement concerns the purely flexural symbol* $\tilde{m}_0(k) = k^2\sqrt{\tanh k/k}$ *at small scaled amplitude; it is not a statement about* $T = \infty$ *at a fixed physical amplitude.*

Taken together, Theorems 4–6 give the phase diagram in Figure 2.

Near T_0 and T_1 the amplitude windows shrink to zero, because the governing indices R and S vanish there; we regard this as structural rather than as a limitation of the method, although the constants could certainly be improved. The windows $(T_0 - 10^{-6}, T_0 + 1.3 \times 10^{-8})$ and $(T_1, T_1 + 3.9 \times 10^{-6})$ are not covered by any of our theorems.

5. Small amplitude: the modulational cluster and the unstable segments

This section proves Theorem 3 and parts (A) and (B) of Theorem 4. All three arguments rest on the same two facts from Section 2: the operator $M = DA$ is real, and $M(-\xi) = -PM(\xi)P$. We write $\lambda = i\mu$, so that instability means a non-real μ.

5.1. The cluster and the structure of its discriminant

At $a = \xi = 0$ the modes $n = -1, 0, 1$ give a triple eigenvalue $\mu = 0$ of M, and every other eigenvalue is at a distance of order one. For complex (a, ξ) in a polydisc $|a| \leq \rho_a$, $|\xi| \leq \rho_\xi$ we certify that exactly three eigenvalues of M lie in $|\mu| < \rho_{\text{cl}}$ and that $M - \mu$ is invertible on the circle $|\mu| = \rho_{\text{cl}}$, by a row-sum (Neumann) test along the homotopy $\operatorname{diag} M + t(M - \operatorname{diag} M)$, $t \in [0, 1]$. The test needs upper bounds for $|m_T(k + \zeta)|$ at complex ζ, which we obtain from interval Taylor-mode automatic differentiation to order 8 at the integers, with a Cauchy

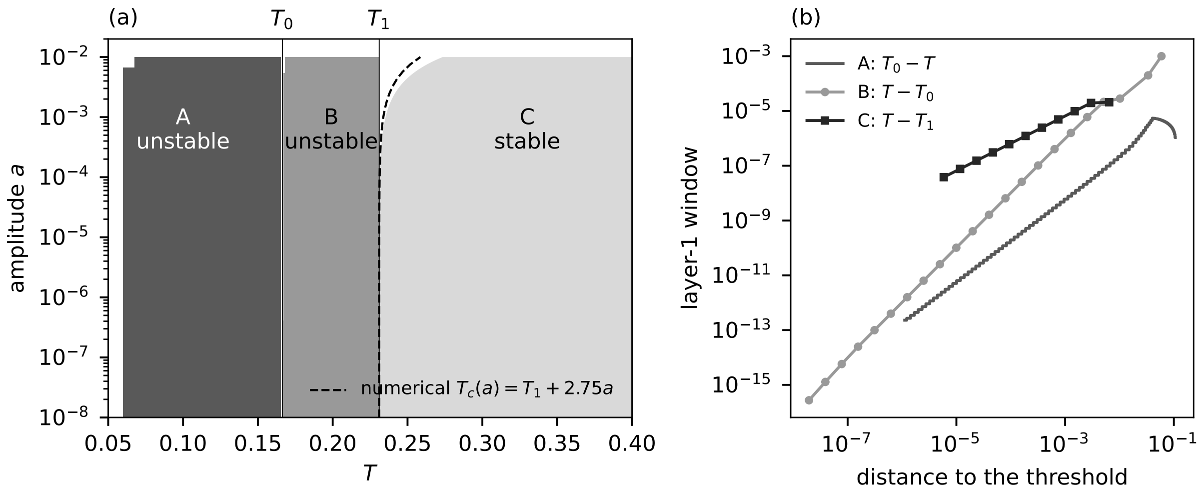

Figure 2: (a) Certified amplitude windows in the (T, a) plane: segment A (modulationally unstable), segment B (sideband unstable) and segment C (spectrally stable for all ξ; the lower bound $\min(10^{-2}, (T - T_1)/4.235)$ is shown). Segment C continues to $T = \infty$ (Theorems 5 and 6). The dashed curve is the numerical finite-amplitude boundary $T_c(a) \approx T_1 + 2.75a$ (a numerical fit, not a theorem). (b) First-layer amplitude windows against the distance to the threshold that bounds them.

bound for the remainder on a disc on which $(1 + Tz^4)\tanh z/z$ has argument in $(-\pi, \pi)$, and for $|k| \geq 14$ from the lower bound $m_T(k) \geq \sqrt{T \tanh 2}\, k^{3/2}$. The wave itself is enclosed for complex a by the same contraction argument as for real a, since that argument uses only moduli. With the cluster isolated, the elementary symmetric functions e_1, e_2, e_3 of its three eigenvalues are analytic in (a, ξ) (by the Riesz projection), and so is the discriminant $\mathrm{Disc} = e_1^2 e_2^2 - 4e_2^3 - 4e_1^3 e_3 + 18 e_1 e_2 e_3 - 27 e_3^2$.

We record three facts used below. (F1) The row-sum test holds for every μ in the closed disc $|\mu| \leq \rho_{\mathrm{cl}}$, not only on its boundary, because the bound used for the complement rows is $|\Lambda_k| - \rho_{\mathrm{cl}}$; hence $M_{QQ} - \mu$ is invertible on the whole disc for Q the modes $|n| \geq 2$, the Schur complement $N(\mu)$ onto $P = \{-1, 0, 1\}$ is analytic in (μ, a, ξ) there, and $F(\mu) = \det(N(\mu) - \mu) = h(\mu) \prod_{i=1}^{3} (\mu_i - \mu)$ with h analytic and zero-free on the disc (its zeros would be further eigenvalues in the disc). (F2) Since $M_{QQ} = D_Q A_{QQ}$ and $D_Q = \mathrm{diag}(n + \xi)$ is invertible on Q, A_{QQ} is invertible as well, so the Schur complement S_A of A onto P is defined and $N(0) = D_P S_A$. (F3) For $|a| \leq A_0$ (complex a included) the normalised wave (even, zero mean, $\hat{f}_1 = a/2$) is the unique fixed point of a contraction on an a priori ball, so it is analytic in a; and since $f(\cdot + \pi)$ is again even, zero-mean and has first coefficient $-a/2$, uniqueness gives $f(z + \pi; a) = f(z; -a)$.

Lemma 7 (divisibility)**.** $\mathrm{Disc}(a, \xi) = \xi^6\, \Phi(a, \xi)$ *with* Φ *analytic on the polydisc, even in* a *and in* ξ*, and real for real arguments.*

Proof. By $M(-\xi) = -PM(\xi)P$ the cluster at $-\xi$ is minus the cluster at ξ, so that e_1 and e_3 are odd and e_2 is even in ξ. At $\xi = 0$ translation invariance gives the Jordan chain $\mathcal{L}_0 f' = 0$, $\mathcal{L}_0 \partial_a f = -(\partial_a c) f'$, so that $\mu = 0$ has algebraic multiplicity at least two, and since $e_1(a, 0) = 0$ the third eigenvalue vanishes as well. Thus $e_2(a, 0) = 0$, and with evenness

$e_2 = O(\xi^2)$. For e_3 we take the Schur complement of $M - \mu$ onto the modes $\{-1, 0, 1\}$, $F(\mu) = \det(N(\mu) - \mu)$. Since $M = DA$, one has $N(0) = D_P S_A$, with S_A the Schur complement of A, hence $F(0) = \xi(\xi^2 - 1)\det S_A$. The function $\det S_A$ is even in ξ (because $A(-\xi) = PA(\xi)P$) and vanishes at $\xi = 0$ (because $A(a, 0)f' = 0$ and f' has nonzero ± 1 components), so that $F(0) = O(\xi^3)$ and $e_3 = -F(0)/h(0) = O(\xi^3)$, with $h(0) \neq 0$ by (F1) and S_A defined by (F2). Substituting into the discriminant gives the factor ξ^6. Evenness in a follows from (F3): the shift $z \mapsto z + \pi$ conjugates the Bloch operators of the waves with amplitudes a and $-a$ (up to the unimodular factor $e^{i\pi\xi}$), so the two clusters coincide. □

The leading part of Φ is computed by the same Schur reduction carried out symbolically. Which data it needs follows from an order count.

Lemma 8 (orders)**.** *(i) $\hat{f}_n(a) = O(a^{|n|})$ for every $n \neq 0$, and $c(a) - m_T(1) = O(a^2)$. (ii) In the scaling $\xi = ta$, $\mu = a\nu$ with t in a compact set, every entry of the 3×3 Schur complement $N(\mu) - \mu$ is $O(a)$, and any change of M of order $O(a^4)$, as well as every contribution of paths through modes $|q| \geq 3$, changes these entries by $O(a^4)$.*

Proof. (i) By (F3) $\hat{f}_n$ and c are analytic in a. Write $\hat{f}_n = \sum_k f_{n,k} a^k$. For $|n| \geq 2$ the wave equation gives $\hat{f}_n(m_T(n) - c) = -\widehat{(f^2)}_n$, with $m_T(n) - c(0) = m_T(n) - m_T(1) \neq 0$ on the range considered ($D > 0$ for $|n| = 2$, and $m_T(n) > m_T(2)$ for $|n| \geq 3$, which is part of the certified wave bounds). The coefficient of a^k in $\widehat{(f^2)}_n$ is a sum of $f_{j,k_1} f_{n-j,k_2}$ with $k_1 + k_2 = k$; by induction on k, $f_{j,k_1} = 0$ for $k_1 < |j|$, so these terms vanish unless $k \geq |j| + |n - j| \geq |n|$, which gives $f_{n,k} = 0$ for $k < |n|$. The statement for c follows from the $n = 1$ equation. (ii) The entries of M are $M_{nm} = (n + \xi)\big((c - m_T(n + \xi))\delta_{nm} - 2\hat{f}_{n-m}\big)$, so an off-diagonal entry is $O(a^{|n-m|})$ by (i); the diagonal entries at $n = \pm 1$ are $O(a)$ (since $c - m_T(\pm 1 + \xi) = O(a^2) + O(\xi)$) and the one at $n = 0$ carries the factor ξ. The complement resolvent is $O(1)$. A path from P to a mode $|q| \geq 3$ and back has total index jump at least 4, hence contributes $O(a^4)$; the same holds for $O(a^4)$ changes of any entry. After the rescaling $\mu = a\nu$, which divides the k-th coefficient of the cubic by a^k, these changes enter the coefficients of the cubic in ν at order a^3, hence the discriminant in ν at order a^3, while Φ only needs the order a^2. □

Consequently the coefficients of Φ at order two use only the wave to order a^2, the symbol to low order around $k = 0, 1, 2$, and the complement modes $|n| = 2$. We kept these data as independent symbols ($m_T'''(1)$, $m_T'(2)$ and the second-order wave coefficient included) and computed Φ in exact arithmetic in the field of rational functions of these symbols. The result is Theorem 3:

$$\Phi = \alpha_6 a^2 + \alpha_8 \xi^2 + O\big((a^2 + \xi^2)^2\big), \qquad \alpha_6 = \frac{2WR^3(2D - R)}{D}, \qquad \alpha_8 = W^2 R^4,$$

in which $m_T'''(1)$, $m_T'(2)$ and the higher wave coefficients cancel identically (`stability_theorem/derive_closed_form_full.py`). Two consistency checks are worth recording. First, $\alpha_6 = R^2 \Delta_{\mathrm{MI}}$ with $\Delta_{\mathrm{MI}} = -2WR(R - 2D)/D$, so that our coefficient is the Hur–Johnson index [6] evaluated on m_T times R^2, although the two were derived along different routes. Second, at $T = 0$ (the gravity Whitham equation with carrier wavenumber $1 < k_c \approx 1.146$) the closed form gives $W, D, 2D - R, R < 0$ and $\alpha_6 > 0$ (modulational stability), consistent with Hur and Johnson [5]. However, an earlier, grid-based version of the statement "$\operatorname{sign}\alpha_6 = \operatorname{sign} R$" missed the condition $W > 0$ and would have failed exactly this check; the closed form is what exposed it.

A real cubic has three real roots if Disc > 0 and one real root and a complex-conjugate pair if Disc < 0. Since $\alpha_8 \geq 0$ always, the sign of Φ near the origin is decided by α_6, and on $T > T_2$, where W, D and $2D - R$ are positive, $\operatorname{sign}\alpha_6 = \operatorname{sign} R$. Thus, on $T_2 < T < T_0$, the cluster is unstable (in a band $|\xi| \lesssim \sqrt{-\alpha_6/\alpha_8}\,|a|$) and real for $T > T_0$, and what remains is to control the remainder.

5.2. Segment A: modulational instability

On each T box in $[0.06, T_0 - 10^{-6}]$ we certify $R < 0$, $W > 0$ and $D > 0$ in interval arithmetic, so that $\alpha_6 < 0 < \alpha_8$, and choose a ray $\xi = \tau a$ with $\alpha_6 + \alpha_8\tau^2 < 0$. Since Φ is even in both variables and bounded by $M_\Phi = 64(\rho_{\mathrm{cl}}/\rho_\xi)^6$ on the polydisc (every difference of two cluster eigenvalues is at most $2\rho_{\mathrm{cl}}$), Cauchy estimates give

$$\Phi(a, \tau a) \leq a^2(\alpha_6 + \alpha_8\tau^2) + \frac{3M_\Phi w^4}{(1-w^2)^2}, \qquad w = |a| \max(1/\rho_a, \tau/\rho_\xi),$$

which is negative for $|a|$ below an explicit threshold. Then Disc < 0 and the cluster has a non-real pair $\mu_{2,3} = x \pm iy$. Writing Disc $= -4y^2|\mu_1 - \mu_2|^4$ and bounding the roots by Fujiwara's bound gives the growth rate $\operatorname{Re}\lambda = y \geq c\,a^2$ with an explicit (and conservative) c. The thresholds are listed in Theorem 4(A). Close to T_0 they decrease like $(T_0 - T)^{3/2}$, because $\alpha_6 \propto R^3$ vanishes there; choosing τ box by box, and not at the centre of the band, is what keeps the exponent at 3/2 instead of 5/2. The ceiling of this route is $a \lesssim \sqrt{|\alpha_6|/M_\Phi}\,\rho_a^2 \sim 10^{-6}$, and it is the reason for the computer-assisted layer of Section 7.

5.3. Segment B: sideband instability

For $T_0 < T \leq T_1$ let $\xi_*(T) \in [-1/2, 0)$ be the collision point of Section 3 between the modes 0 and 1, $\Omega(\xi_*) = \Omega(1 + \xi_*) =: \omega$, and $\kappa = \sqrt{|\xi_*|(1 + \xi_*)}$. With P the projection onto $\{0, 1\}$ and $\lambda = i\omega + z$, the leading 2×2 block has determinant $z^2 + a^2\xi_*(1 + \xi_*) = z^2 - a^2\kappa^2$, whose roots $z = \pm a\kappa$ are real. The proof is a Feshbach reduction with remainder control.

1. *Complement.* On ℓ^1 the zero-amplitude complement is diagonal with entries $\Omega(n + \xi) - \omega$, $n \notin \{0, 1\}$, and we certify their minimum $\delta_{\min}$ (for $|n| \leq 8$ directly, beyond by the lower bound on m_T). The perturbation $\mathcal{L} - \mathcal{L}_0$ is then small in the resolvent norm, so the complement resolvent is bounded by a Neumann series.
2. *The mode $n = -1$.* Its gap to the colliding pair is the second difference $\Psi(1 + \xi) + \Psi(1 - \xi) - 2\Psi(1)$, three terms of size ~ 0.95 that cancel to ~ 0.004. A direct interval evaluation over a wide ξ enclosure loses the cancellation, and so does the mean-value form $\xi^2\Psi''(\theta)$. We resolve it by subdividing T so finely (boxes of width $\sim 2 \times 10^{-5}$) that the enclosure of $\xi_*(T)$ becomes narrow enough for a direct evaluation, or, on the extended range, by the enclosure $\xi^2 \min \Psi''$.
3. *Schur remainder.* The row $n = 0$ of $\mathcal{L}_\xi$ carries the factor ξ (because $(\partial_z + i\xi)$ acts on the zero mode as multiplication by $i\xi$), so that the path through $n = -1$ contributes only $|\xi|a^2/\delta_{-1}$. This refinement raised the amplitude threshold on $[0.18, 0.22]$ from 3.5×10^{-6} to 1.99×10^{-4}.

4. *Rouché.* On the circle $|z - a\kappa| = a\kappa/2$ the reference determinant dominates all corrections, so one eigenvalue lies in the disc, and $\operatorname{Re}\lambda \geq |a|\kappa/2$.

The travelling wave on this range is enclosed by the same contraction argument as elsewhere, with the weighted norm $\|f\|_{W,1} = \sum |m||\hat{f}_m|$ bounded directly (an earlier version used an inequality $|m_T(n) - c| \geq 0.4165\, n^{3/2}$, which fails at $n = 2$; the corrected constants change the thresholds only in the fifth digit). We ran the argument on 22 consecutive T slabs, obtaining the thresholds of Theorem 4(B).

The two ends of segment B behave differently, and the difference is physical. At the upper end $\xi_* \to -1/2$ and $\kappa \to 1/2$, the nearest complement modes stay far away, and at $T = T_1$ itself the block reduces to $\left(\begin{smallmatrix} 0 & a/2 \\ -a/2 & 0 \end{smallmatrix}\right)$, which gives the real growth rate $a/2$; the only complication is that ξ_* becomes a tangency, and there we locate it by the intermediate value theorem using $S(T) \leq 0$ and the certified monotonicity $S' > 0$. Thus the instability extends to T_1 with a uniform amplitude threshold 10^{-3}. At the lower end $\xi_* \approx -2R/W \to 0$, $\kappa \propto \sqrt{T - T_0}$ and the gap to $n = -1$ closes like $W\xi_*^2$, so that the sideband collision merges into the modulational cluster; the certified threshold decreases like $2.3(T - T_0)^2$ down to $T - T_0 \approx 10^{-7}$ (on the last three slabs the certified constant falls to ~ 1.6), and we stop at $T - T_0 = 1.3 \times 10^{-8}$; the interval $(T_0, T_0 + 1.3 \times 10^{-8})$ is not covered.

6. Small amplitude: the stable segment

On the stable segment every eigenvalue of every $\mathcal{L}_\xi$ has to be accounted for, and the arguments split the Bloch parameter into three ranges: an outer region $0.05 \leq |\xi| \leq 1/2$, where all zero-amplitude eigenvalues are simple and separated; a middle band $\kappa|a| \leq |\xi| \leq 0.05$, where the three cluster eigenvalues are distinct but close; and the band core $|\xi| \leq \kappa|a|$, where the cluster is a perturbed Jordan block and stability is the sign of the discriminant of Section 5.1. In each range the conclusion comes from the same symmetry: an eigenvalue that is alone in a region invariant under $\mu \mapsto \bar{\mu}$ is real. By $M(-\xi) = -PM(\xi)P$ it suffices to take $\xi \geq 0$.

6.1. The outer region (Theorem I)

Let $\Omega_n = \Omega(n + \xi)$ be the zero-amplitude eigenvalues. For $T > T_1$ there are no collisions, and we certify a uniform lower bound g for the gaps between neighbouring Ω_n over the whole (T, ξ) region. Three pairs are delicate, namely $(-1, 0)$, $(0, 1)$ and $(-1, 1)$, because each gap is a near cancellation of order-one terms (the last is again the second difference $\Psi(1 + \xi) + \Psi(1 - \xi) - 2\Psi(1)$). A uniform grid fine enough to resolve them would need $\sim 3 \times 10^6$ boxes in (T, ξ), whereas a branch-and-bound that refines only near the minimum closes with $\sim 9 \times 10^4$ nodes and gives $g \geq 0.0018$ on $[0.24, 0.70]$. Around each Ω_n we take a disc D_n centred on the real axis, with radius set by the nearest neighbour gap for the near modes and by the monotone gap of Ψ for the far modes, and we check that the discs are pairwise disjoint. In the ℓ^1 (Wiener) norm, $(\operatorname{diag} M - \mu)^{-1}$ is diagonal and the perturbation $V = M - \operatorname{diag} M$ satisfies $\|V(\operatorname{diag} M - \mu)^{-1}\| \leq q < 1$ outside all discs, with $q = 0.278$. Along the homotopy $\operatorname{diag} M + tV$ no eigenvalue crosses a disc boundary, so each D_n contains exactly one eigenvalue, which is therefore real. The wave enters only through the bounds $\|v\|_W \leq 3.71a^2$, $\|v\|_{W,1} \leq 3.71a^2$ and $|c - m_T(1)| \leq 7.41a^2$ for $v = f - a\cos z$, obtained from a contraction argument in the Wiener algebra, and the result holds for $|a| \le 5 \times 10^{-5}$ (certified up to 8.99×10^{-5}).

This argument uses neither Krein signatures nor a determinant, only simplicity and the symmetry of the spectrum. In the audit described in Appendix Appendix B two steps of an earlier version were tightened: the tail gap was evaluated only at the first tail mode, and the disc radii for far modes were not specified; both are now bounds valid outside all discs, with the radii written out and checked.

6.2. The middle band (Theorem J)

For $\kappa|a| \le \xi \le 0.05$ (with $\kappa = 12$ on $[0.24, 0.70]$) the pair $\Omega_{\pm 1}$ is separated by $\approx W\xi^2$ and the mode 0 lies at a distance $\approx R\xi$ from it, while the amplitude corrections are $O(a^2)$. We first count eigenvalues globally: a cluster disc $|\mu| \le 0.08$ contains exactly three eigenvalues and each mode $|n| \ge 2$ has its own real-centred disc with one eigenvalue, by the same homotopy argument with a row-sum bound ≤ 0.0051. This step also proves that all non-cluster eigenvalues are real for every $|\xi| \le 0.05$, a point that the band-core analysis alone does not address. We then take the Schur complement onto $\{-1, 1\}$ with every other mode, *including* $n = 0$, in the complement. Since the whole row $n = 0$ of M carries the factor ξ, eliminating $n = 0$ costs only $O(a^2/R)$ and not $O(a^2/(R\xi))$. Rouché's theorem on two real-centred discs of radius $0.45\, g_{\rm lo}$ around $\Omega_{\pm 1}$, $g_{\rm lo} = \xi^2 \min \Psi'' - O(a^2)$, then places one real eigenvalue in each, provided $(a/\xi)^2$ is below an explicit constant; that is where the condition $\xi \ge \kappa|a|$ comes from. The third cluster eigenvalue is real by conjugation symmetry. As a falsification test we ran the same certificate at $T = 0.13$, where the modulational band exists: direct diagonalisation puts the band edge at $11.5a$–$12a$ (the closed form predicts $11.7a$), and the certificate would need $\kappa \approx 21.6$ there, so it does not certify a false statement.

6.3. The band core (Theorems K and K$^+$)

For $|a|$ and $|\xi|$ both small the cluster is governed by Lemma 7, and on $T > T_0$ the leading part $\alpha_6 a^2 + \alpha_8 \xi^2$ of Φ is positive definite. We enclose α_6 and α_8 on each T box from their closed forms, which involve only R, W and D and therefore do not suffer from the dependency problem that makes an interval evaluation of the whole Schur reduction useless. If $|\Phi| \le M$ on the polydisc, evenness gives for the part of degree ≥ 4

$$|E| \le \frac{3Mw^4}{(1 - w^2)^2}, \qquad w = \max(|a|/\rho_a, |\xi|/\rho_\xi),$$

and $|E| < \min(\alpha_6 \rho_a^2, \alpha_8 \rho_\xi^2)\, w^2$ implies $\Phi > 0$, hence $\mathrm{Disc} > 0$ and three distinct real cluster eigenvalues. Everything therefore depends on M.

Theorem K takes $M = 64(\rho_{\rm cl}/\rho_\xi)^6$ from the certified cluster radius and gives $|a| \le 1.89 \times 10^{-6}$, $|\xi| \le 1.89 \times 10^{-5}$ on $[0.24, 0.70]$. This bound only uses that each difference of two cluster eigenvalues is at most $2\rho_{\rm cl}$, whereas the actual differences are $\sim 0.78\xi^2$ for the ± 1 pair and $\sim 0.3|\xi|$ for the third eigenvalue, so it overestimates by a factor 10^4–10^5. Theorem K$^+$ replaces it by a rigorous bound for $\sup|\Phi|$ on the torus $|a| = \rho_a$, $|\xi| = \rho_\xi$ (by the maximum principle this bounds Φ on the polydisc, and on the torus $|\Phi| = |\mathrm{Disc}|/\rho_\xi^6$). The torus is reduced by the symmetries $a \mapsto -a$, $\xi \mapsto -\xi$ and complex conjugation to a quarter, covered by complex balls, and on each ball:

- the complex-amplitude wave is enclosed by a ball fixed point inside the a priori ball on which the contraction was proved;
- the diagonal entries $c - m_T(n+\xi)$ are evaluated as $(c - m_T(1)) + (m_T(1) - m_T(n)) - (m_T(n+\xi) - m_T(n))$, with a mean-value form in T for the second bracket and a Taylor series of degree 12 in ξ with a Cauchy remainder for the third; evaluated directly, ball arithmetic loses the correlation in T and the radii grow by a factor ~ 10;
- the three cluster eigenvalues are enclosed by column Gershgorin discs in a numerical eigenbasis, isolated from all other discs (including those of the tail modes), and $|\mathrm{Disc}| = \prod_{i<j} |\mu_i - \mu_j|^2$ is bounded from the overlap pattern of the three discs, with $d_{ij} = |c_i - c_j| + r_i + r_j$: the product $\prod d_{ij}$ bounds $\prod |\mu_i - \mu_j|$ when the discs are disjoint, $\max(d_{ij}, d_{ik})^2\, D_{jk}$ when only the pair (j,k) may overlap, with $D_{jk} = \max(d_{jk}, 2r_j, 2r_k)$ the diameter of the union (which covers the case of one disc nested in the other), and the cube of the diameter of the union when all three may merge; $|\mathrm{Disc}|$ is bounded by the square.

On $[0.24, 0.70]$ this gives $\sup|\Phi| \le 5.34 \times 10^{-4}$ on the binding box (against 6.7 from Theorem K), $a_{K^+} = 2.1 \times 10^{-4}$ and $\xi_{K^+} = 1.09 \times 10^{-3}$, so that the band core joins Theorem J for every $|a| \le 5 \times 10^{-5}$ (the scope of Theorem J itself).

We record one error found in this step, because it passed a first round of checks. In the first version of the overlap test the inequality was reversed, so that separated discs were sent to the (valid but loose) cube bound and overlapping discs to the product formula, although that formula is not valid for them. All results of that version were withdrawn and recomputed; the numbers above are from the corrected code, and the audit of Appendix Appendix B added the union-diameter case for nested discs.

6.4. Up to T_1, and up to $T = 10$

Close to T_1 the smallest zero-amplitude gap is $S(T) \approx 0.363(T - T_1)$, attained by the pair $(-1, 0)$ at $\xi = 1/2$, where the sideband collision takes place for $T < T_1$. Theorem I needs the amplitude to be small compared with this gap, so its threshold must shrink linearly, and this is not a weakness of the method: by Theorem 4(B) the instability persists up to T_1 with a uniform threshold, and numerically it appears to persist to $T \approx T_1 + 2.75a$ at finite amplitude (Section 9). We ran Theorem I on 11 slabs halving $T - T_1$ down to 3.9×10^{-6}, with gap target $0.9\, S(T_{\mathrm{lo}})$ and amplitude 0.03 times that target; the slab runner executes the original proof unchanged except for these parameters (and reproduces the default run to the last digit, on two versions of the interval library). The band core and middle band need only $R, W, D > 0$ and were run on the strip $(T_1, 0.24)$ in one piece. The amplitude thresholds are $\approx 0.01(T - T_1)$ near T_1, 3.8×10^{-8} on the last slab, and ~ 1.2–1.6×10^{-6} for $T - T_1 \ge 1.25 \times 10^{-4}$.

For $T \in [0.70, 10]$ the same three theorems apply with a larger cluster radius (the cluster grows like $\sqrt{T}$) and, for $T \ge 1.5$, a larger amplitude radius $\rho_a = 0.049$ in Theorem K$^+$, which is admissible because the contraction constant of the wave map improves with T. Theorem J is run with $\kappa = 4$ (the value actually needed is between 0.81 and 3.3). The join between the three pieces is 3×10^{-4}, 9.9×10^{-4} and 6×10^{-4} on $[0.70, 1.5]$, $[1.5, 4]$ and $[4, 10]$, respectively, and the outer region is covered by Theorem I for $|a| \le 5 \times 10^{-5}$. This proves Theorem 4(C) on $[T_1 + 3.9 \times 10^{-6}, 10]$; the range $T \ge 10$ is Section 8.

7. The computer-assisted layer

The first layer stops at amplitudes of 10^{-6} to 10^{-3}, because it is built on power series in (a, ξ) whose remainders are controlled by Cauchy estimates on a polydisc of radius $\rho_a \lesssim 0.05$. To reach $a = 10^{-2}$ we compute at finite amplitude directly, on boxes in (T, a) (and, for the stable segment, in ξ), in ball arithmetic (Arb through python-flint, 192 bits), with floating point used only to produce centres and guesses. This section describes the common ingredients, then the certificates for the unstable and the stable segments, and finally how the boxes are assembled into Theorem 5.

7.1. Common ingredients

First-order Taylor models. Every quantity on a box is written as $x(p) = x_0 + x_T\,\delta T + x_a\,\delta a + e$, $|e| \le r$, with the linear part carried exactly and only second-order effects in the remainder. This is what makes boxes of useful size possible. On segment A, for example, the two unstable eigenvalues are separated by $\sim a^2$ but drift with T by $\sim a\,\delta T$; with a constant-plus-radius enclosure the drift would enter $\operatorname{Re}\lambda$, whereas the linear part absorbs it.

The travelling wave. From a numerical centre and its parameter derivatives we form a candidate set $\mathcal{V} = \bar{v} + \bar{v}_T\delta T + \bar{v}_a\delta a + B(r)$, including an ℓ^1 tail mass and a weighted tail, and verify that the fixed-point map of (2) (in the form $\hat{v}_n = -\widehat{(f^2)}_n/(m_T(n) - c)$, $|n| \ge 2$, with c fixed by the $n = 1$ equation) maps $\mathcal{V}$ into itself. The radius is iterated to self-consistency and not prescribed, because the error in c is amplified by $1/(m_T(n) - c)$. A separate Lipschitz bound shows that the map is a contraction on the a priori ball $\|v\| \le 2a^2/g$, so that the fixed point in $\mathcal{V}$ is the wave. The wave speed is written as $c = m_T(1) + 2\hat{v}_2 + (4/a)\sum_k \hat{v}_k\hat{v}_{k+1}$, which avoids dividing an $O(a^3)$ quantity by a.

Truncation and tail. The Bloch matrix is truncated to $|n| \le 12$ (25 modes), each entry a Taylor model. The complement $\{|m| > 12\}$ is handled by a Schur complement whose entries are bounded through a Neumann series in the column-sum (ℓ^1) norm, including the weighted wave norm; lower bounds for the tail diagonal use the growth of m_T with explicit constants (for complex ξ we use $|m_T(z)|^2 \ge (Tu^3 - 1/u)\tanh u$, $u = \operatorname{Re} z$, which the audit required in place of an unproved monotonicity).

7.2. Unstable segments

On segment A we fix the fibre $\xi = \tau a$ (with τ chosen by a numerical scan at the box centre, which is not part of the proof), and on segment B the fibre follows the collision point, $\xi = \xi_*(T_c) + \xi_*'(T_c)(T - T_c)$. The unknowns are $x = (\mu, \varphi_{n\ne j_0})$ with $M\varphi = \mu\varphi$ and $\varphi_{j_0} = 1$, and the tail enters $F(x, p) = 0$ through the Schur complement and its μ-derivative, as radii. We use a parametrised Krawczyk operator with a moving centre $\tilde{x}(p) = x_0 + x_T\delta T + x_a\delta a$ (the linear part from the implicit function theorem) and verify, componentwise and for every p in the box,

$$|A\,F(\tilde{x}(p), p)| + |I - A\,DF(X_p, p)|\,r < r, \qquad X_p = \tilde{x}(p) + B(r),$$

together with the condition that the eigenvalue enclosure lies in the disc assumed by the tail bound. Then $F(\cdot, p)$ has a unique zero in X_p, and with $\lambda = i\mu$ we bound $\operatorname{Re}\lambda = -\operatorname{Im}\mu$ from below by treating the real and imaginary parts of the linear coefficients separately. A fixed centre was tried first and fails, since the zero drifts out of a ball around it.

We ran about 1.66×10^6 tasks for the first cover and 4.9×10^6 for a second pass that closed the gap $[0.1591, 0.16516]$ in segment A. Every task that did not certify lies either near T_2 at large amplitude, where the modulational instability is absent at finite amplitude (Section 9), or in the degenerate neighbourhoods of T_0. Results on a compute node and on a laptop agreed bit for bit. As a sanity check, at $T = 0.13$, $a = 10^{-2}$ the certificate gives $\operatorname{Re}\lambda \geq 15.3a^2$ against $14.8a^2$ from the numerical Floquet computation (at a slightly different τ), and at $T = 0.20$, $a = 10^{-2}$ it gives 3.79×10^{-3}, the leading-order value $a\kappa$ with $\kappa = 0.384$.

7.3. The stable segment: outer region

For $\xi \in [0.045, 1/2]$ we show that M has real spectrum by column Gershgorin discs in a numerical eigenbasis. Let V be the real numerical eigenvectors of the truncated matrix at the box centre, and $K = V^{-1}MV$ on the modes $|n| \leq 12$, the identity on the tail. The P-column discs have radii from the off-diagonal column sums plus the tail rows; the tail discs are centred at $\Lambda_m = (m + \xi)(c - m_T(m + \xi))$ with radii from the wave norms. We check that the P discs are pairwise disjoint, that they avoid the innermost tail discs (with the sign of Λ_m taken into account), and that consecutive tail discs are disjoint, using a lower bound for Ψ' that is increasing beyond an explicit wavenumber. A homotopy then gives exactly one eigenvalue per disc, and since K is real and every disc is centred on the real axis, each eigenvalue is real.

7.4. The stable segment: band core

For $\xi \in [0, 0.05]$ the difficulty is structural. At $a = \xi = 0$ the ± 1 pair of the scaled problem below is a Jordan block, its roots at finite (a, ξ) are $d \pm \sqrt{\varepsilon}$ with $\varepsilon \propto \Phi(a, \xi)$, and stability is the sign of an $O(a^2)$ quantity. Any finite-amplitude evaluation has to resolve it, so with first-order Taylor models the boxes are $\sim a$ wide and the cost grows like $1/a$ (the same reason makes the segment A boxes $\sim a$ wide). We remove the two exact degeneracies first.

- *The factor ξ.* For $\xi \notin \mathbb{Z}$, $M\varphi = \xi\nu\varphi$ is equivalent to $A\varphi = \nu E\varphi$ with $E = \xi D^{-1} = \operatorname{diag}(1 \text{ at } n = 0,\ \xi/(n + \xi) \text{ otherwise})$.
- *The translation mode.* With $g_n = n\hat{f}_n$ the wave equation gives $A(0)g = 0$ exactly, and since $A(\xi) - A(0) = -\operatorname{diag}(m_T(n + \xi) - m_T(n))$ one has $(A - \nu E)g = \xi w$ and $g^{\mathsf{T}}(A - \nu E)g = \xi^2\tau$ with explicit w and τ (pairing the terms $\pm n$ produces the second factor ξ). A congruence that replaces the first unit vector by g, followed by a rescaling of that slot by $1/(a\xi)$, yields a real symmetric pencil $Q(\nu, \xi) = Q_0 - \nu Q_1$ that is analytic at $\xi = 0$ and whose zeros are the scaled eigenvalues. The transformation, the determinant relation $\det Q = \det(A - \nu E)/(4\xi^2)$ and the cancellation of all $1/a$, $1/\xi$ factors are written out in Appendix Appendix A.

The divided differences in w and τ are enclosed by Taylor polynomials in ξ (degree 12) with Cauchy remainders on discs $|z - n| = 0.4$, on which m_T is analytic and zero-free for $n \geq 1$. The certificate on one box then has three steps: a block column-Gershgorin count shows that a cluster disc holds exactly three eigenvalues and every other disc exactly one real eigenvalue; the 3×3 Schur complement of the pencil onto $\{e_{-1}, e_0, \text{slot}\}$, after an orthogonal congruence by the centre eigenvectors (with $\det U \neq 0$ certified), changes sign at four ordered test points

$\nu_1 < \cdots < \nu_4$ that move linearly with the parameters, while the complementary block is certified invertible on the whole interval $[\nu_1, \nu_4]$; and a distance check identifies the three real zeros found in this way with the three cluster eigenvalues. At $\xi = 0$ the cluster is real by continuity, and $\xi < 0$ follows by symmetry. The $n = 0$ diagonal entry is a real first-order Taylor model valid for every $T > 0$, and Cauchy discs are used only for $n \geq 1$, where the roots of $1 + Tz^4$ stay at distance $\geq \sin(\pi/4)$ from the integers; this is why the same code applies without change for large T (Section 8).

7.5. Coverage and provenance

Each batch consists of a task file of parameter boxes and the leaf records written by the runner, which bisects failed boxes to a fixed depth. Box endpoints are rounded to 20 decimal digits before use, the certified half-widths are enlarged by a relative 10^{-25} so that neighbouring boxes overlap, and the coverage check compares endpoints as exact rationals. After the audit, the coverage checker requires, for every task, that its leaves cover the full (T, a, ξ) box, that the leaf kind equals the task kind, that task identifiers equal their positions, and that every code hash recorded in a leaf is present, and re-hashes correctly, in an archive of the proof code; in addition, the assemblies require that the set of code manifests seen in each batch equals exactly the one approved manifest for that batch, so that a leaf produced by an archived but superseded version is rejected; the reports record the hashes of the task file and of the ordered leaf files, and the assembly scripts refuse a report whose task-file hash differs from the file they read. Negative tests (a stale hash, a missing code file, a wrong kind, a leaf outside its task, a partial leaf, identifiers that are not positions, a same-count substitution, and a report carrying a different approved manifest) are all rejected.

The assembly for Theorem 5(C) computes, for every T, the end $a^*(T)$ of the contiguous amplitude range from 0 that is covered by layer 1 or by the intersection of the outer and band-core covers, and checks $a^*(T) \geq \min(10^{-2}, (T - T_1)/4.235)$ at every breakpoint. The batches are listed in Table 1.

batch	region	tasks	status
D1–D4, D5	segments A, B	1.66×10^6; 4.93×10^6	certified (A: $[0.0675, 0.16516]$; B: $[0.1681, T_1]$)
CO	C, outer, $T \leq 0.70$	4,267	all covered
CK, CK2	C, core, $a \in [10^{-5}, 10^{-2}]$	66,178; 608,258	all covered
SO, SK, SO2, SK2	C, strip $(T_1, 0.24)$	647; 18,007; 59; 1,564	all covered
BO, BK1–BK3	C, $T \in [0.70, 10]$	5,301; 91,296; 117,100; 434,040	all covered
T10 (O, K)	C, $T \in [10, 473]$	4,408; 12,029	all covered

Table 1: Batches of the computer-assisted layer and their numbers of tasks (each task is a box in (T, a, ξ), subdivided adaptively into leaves).

8. Large rigidity and the flexural limit

8.1. Rescaling

For large T the symbol is dominated by the bending term, and the natural variables are $\delta = T^{-1/2}$, $m_T = \sqrt{T}\,\tilde m_\delta$, $u = \sqrt{T}\,\tilde u$ with time rescaled by $\sqrt{T}$, where

$$\tilde m_\delta(k) = \sqrt{(\delta^2 + k^4)\,\frac{\tanh k}{k}}.$$

The travelling-wave problem and the Bloch operators keep their form with $\tilde m_\delta$ in place of m_T, and the amplitude becomes $\tilde a = a\delta$. The physical target $0 < a \le 10^{-2}$ is thus the wedge $0 < \tilde a \le 10^{-2}\delta$, which closes at $\delta = 0$. The range $T \ge 10$ corresponds to $\delta \in [0, 10^{-1/2}]$, a compact interval, and $\delta = 0$ gives the purely flexural symbol $\tilde m_0(k) = k^2\sqrt{\tanh k/k}$. Numerically the spectrum stays exactly real on this whole range (for $\tilde a$ up to 0.1 at $\delta = 0$), and the minimal zero-amplitude gap scales like $\sqrt{T}$, so that no new mechanism appears.

8.2. The branch point at $n = 0$ and the θ-lift

Only one entry is not analytic uniformly in δ: the $n = 0$ symbol $\tilde m_\delta(\xi) = s(\xi)\sqrt{\delta^2 + \xi^4}$, $s(\xi) = \sqrt{\tanh \xi/\xi}$, whose analyticity radius in ξ is $\sim \delta^{1/2}$ and vanishes as $T \to \infty$. Every other entry, and the wave itself (which involves only $\tilde m_\delta(j)$, $j \ge 1$), is analytic in (ξ, δ) uniformly on $\delta \in [0, 10^{-1/2}]$. The complex ξ-balls of Theorem K$^+$ are therefore the only place where the first layer breaks down as $T \to \infty$. We remove the branch point by writing, for real δ and ξ,

$$\sqrt{\delta^2 + \xi^4} = \delta + \theta\,\xi^2, \qquad \theta = \frac{\xi^2}{\sqrt{\delta^2 + \xi^4} + \delta} \in [0, 1],$$

and treating θ as an independent real parameter. For fixed (δ, θ) the lifted symbol $s(\xi)(\delta + \theta\xi^2)$ is even and analytic in ξ with radius $\pi/2$, and every physical point lies in the lifted family. Theorem K$^+$ is run with δ and θ as real interval parameters and the complex torus in $(\tilde a, \xi)$ as before. The closed form of Theorem 3 survives the lift: with the $n = 0$ symbol replaced by $d_0 + p_2\xi^2 + p_4\xi^4$ and all three coefficients symbolic, the identities $\alpha_6 = 2WR^3(2D - R)/D$ and $\alpha_8 = W^2R^4$ hold exactly, with $R = \tilde m(1) - d_0 + \tilde m'(1)$ (`derive_closed_form_lifted.py`). In interval arithmetic, on $\delta \in [0, 10^{-1/2}]$, $R > 2.057$, $W > 4.04$, $D > 1.87$ and $2D - R > 1.386$, so that the band core is uniformly nondegenerate.

8.3. The first layer, uniformly in δ

With these changes the three pieces of Section 6 hold uniformly on $\delta \in [0, 0.3163]$, in the scaled amplitude: Theorem I with gap target 0.0095 for $|\tilde a| \le 4.6 \times 10^{-4}$ (a branch-and-bound with 2.2×10^5 nodes, certified up to 4.74×10^{-4}), Theorem J with $\kappa = 2.5$ (the value needed is 2.22) for $|\tilde a| \le 1.1 \times 10^{-3}$, and Theorem K$^+$ with $\rho_a = 0.049$ over the full range $\theta \in [0, 1]$, giving $\tilde a_K = 2.7 \times 10^{-3}$ and $\xi_K = 2.78 \times 10^{-3}$. The binding piece is Theorem I, whose radius is about 1/20 of the gap; the true scaled minimum gap is ≈ 0.010, and the target 0.0099 does not close. This proves Theorem 6: $|\tilde a| \le 4.6 \times 10^{-4}$ uniformly in δ, and hence the physical target $a \le 10^{-2}$ for $10^{-2}\delta \le 4.6 \times 10^{-4}$, that is, $T \ge T^* = 472.6$.

8.4. The second layer on $[10, 473]$

The remaining region is $T \in [10, 473]$, $a \in [4.6 \times 10^{-4}\sqrt{T}, 10^{-2}]$, the complement of the first layer in physical units. An audit of the finite-amplitude code shows that no step uses analyticity of the $n = 0$ symbol or an upper bound on T: the $n = 0$ entry is a real Taylor model, Cauchy discs are used only for $n \geq 1$, the tail constants use only Tk^3-type lower bounds that improve with T, and the separation of the tail discs requires $u^4 > 3/T$. The code of the $[0.70, 10]$ batches is therefore used unchanged (same hashes). Sizing runs certify outer-region tasks of T width $T/100$ directly, and band-core tasks of T width $0.8\,aT$ with at most four levels of subdivision; one band-core task costs from ~ 11 CPU minutes at $T = 20$ to ~ 5 CPU hours at $T = 470$. The production batch has 16,437 tasks. All 16,437 tasks are certified and cover their boxes exactly (`check_C_coverage.py`), every leaf carries the hashes of the approved code, and the assembly `check_C_T10plus.py` verifies that the certified set, together with the first layer, contains $0 < a \leq 10^{-2}$ for every $T \in [10, 473]$ and that the first layer alone covers $0 < a \leq 10^{-2}$ for $T \geq 473$. This completes Theorem 5(C) for all $T \geq 0.231082819472$.

9. Comparison with numerical computations

The statements in this section are numerical (floating point, Fourier truncation), not proofs. We include them because they show where our theorems sit in the larger picture computed by Flamarion and Adriazola [2], and because they suggest a mechanism behind some of their observations.

9.1. The numerical code and its benchmarks

Waves are computed by Newton's method in Fourier space, either with the amplitude a fixed (as in the rest of this paper) or with the height $H = f(0) - f(\pi)$ fixed (as in [2]), and the Bloch spectrum by the Fourier–Floquet–Hill method [12] on the truncated matrix $M = DA$, with instability detected as a non-real eigenvalue of this real matrix. We benchmark the code in three ways. The gravity Whitham equation with carrier wavenumber κ must be modulationally stable for $\kappa < k_c \approx 1.146$ [5], and the code reproduces this threshold sharply (growth rates at the level of rounding for $\kappa \leq 1.1455$, and $0.088a^2$, $0.47a^2$, $0.91a^2$ at $\kappa = 1.2, 1.5, 2$). KdV cnoidal waves are spectrally stable, and the code finds no instability. Finally, translation invariance requires $\mathcal{L}_0 f' = 0$, which the code satisfies to $\sim 10^{-21}$ in high precision. However, an earlier version of the code passed its own residual test while solving the wrong equation (a reversed convolution index, used in both the solver and the residual), and reported instability for every $T > T_1$; only the benchmarks above exposed it. With 128 wave modes and Bloch truncation $|n| \leq 80$ the numbers below agree to all printed digits with 64 and 48, respectively.

9.2. Agreement with Flamarion and Adriazola

Table 2 lists the maximal growth rate over ξ at the rigidities of their Figure 8. Read against their Figures 1, 5, 6 and 8 (to the accuracy of reading a plot, ~ 0.005), the two computations agree: at $T = 0.10$ the growth rate rises to ~ 0.025 near $H = 0.15$ and vanishes from $H \approx 0.3$ on (their "complete stabilisation"); at $T = 0.20$ it increases monotonically to ~ 0.07; at $T = 0.45$ small waves are stable, instability sets in near $H = 0.2$, and the growth rate reaches ~ 0.08 at $H = 0.5$; at $T = 0.80$ and 1.00 every wave is stable. For $T = 0$ we find the onset between $H = 0.25$ and 0.30 (theirs ≈ 0.30) and growth rates of 0.0047, 0.014 and 0.036 at $H = 0.35$, 0.40 and 0.45, against loops of ~ 0.005, ~ 0.013 and ~ 0.04 in their Figure 1.

$T\backslash H$	0.05	0.10	0.15	0.20	0.25	0.30	0.35	0.40	0.45	0.50
0.10	0.0066	0.0214	0.0248	0.0218	0.0129	0	0	0	0	0
0.20	0.0119	0.0249	0.0359	0.0452	0.0527	0.0585	0.0629	0.0661	0.0681	0.0694
0.45	0	0	0	0.0134	0.0321	0.0448	0.0556	0.0653	0.0740	0.0820
0.80	0	0	0	0	0	0	0	0	0	0
1.00	0	0	0	0	0	0	0	0	0	0

Table 2: Numerical maximal growth rate $\max_\xi \operatorname{Re}\lambda$ against the height H, at the rigidities of [2, Fig. 8]. Every nonzero entry has its maximum at $\xi = 1/2$, except $T = 0.10$, $H = 0.05$, where it is at $\xi = 0.241$ (the modulational band). A zero means that the computed spectrum is real.

9.3. What the Bloch parameter adds

Flamarion and Adriazola describe their instabilities for $0.1 < T \leq 0.7$ as modulational. Our computations suggest a different reading. In every unstable entry of Table 2 with $T \geq 0.1$ and $H \geq 0.1$ the maximal growth is at the band edge $\xi = 1/2$, so that it likely comes from the pair of modes $(-1, 0)$, the sideband collision of Section 3. At small amplitude this collision exists only for $T_0 < T \leq T_1$; at finite amplitude it survives to larger T, and its boundary moves like

$$T_c(a) \approx T_1 + 2.75a, \qquad \text{i.e.} \qquad S(T_c) \approx a - 4.7a^2,$$

a numerical fit to bisections in T at $a = 10^{-4}, 10^{-3}, 10^{-2}$, where $(T_c - T_1)/a = 2.750$, 2.740, 2.655 (we have not derived the correction term). To leading order this is the 2×2 Krein test $|S| < a$ at $\xi = 1/2$, with $\kappa = 1/2$. For larger heights the onset of instability at $\xi = 1/2$ is at $H \approx 0.06$, 0.20, 0.34, 0.44 and 0.48 for $T = 0.30$, 0.45, 0.60, 0.70 and 0.75, and it passes $H = 0.5$ near $T \approx 0.76$. This is consistent with the cut-off near $T = 0.7$ in their Figure 8, which covers heights up to 0.5 and the rigidities 0.45, 0.80 and 1.00 in this range. Thus the regime "stable for small H, unstable for larger H" is, in our reading, a band-edge instability boundary $T_c(H)$ crossing the given T, consistent with (but not proved to be) the continuation of the sideband collision; confirming the identification would require tracking the eigenpair and its mode content continuously in (a, T), and the stable regime they find for $T > 0.7$ is the region above this boundary within their range of heights. We have not followed the boundary beyond $H = 0.5$, so that we cannot rule out instability of higher waves at $T > 0.76$.

Instabilities away from the origin of the Bloch circle have been computed before for related scalar and Whitham-type models, e.g. for the gravity and capillary Whitham equations [11, 13] and, by a perturbative collision analysis, for a Boussinesq–Whitham system [14]; in the water-wave literature the band-edge case $\xi = 1/2$ is also called subharmonic or period-doubling. Two further observations are consistent with this picture. First, at $T = 0.10 < T_0$ the maximum moves from the modulational band ($\xi = 0.241$ at $H = 0.05$) to $\xi = 1/2$ from $H = 0.10$ on. The single finite-amplitude certificate that we built at the start of this project

($T = 0.1$, $H = 0.05$, $\operatorname{Re}\lambda > 0.006626$ for $\xi \in [0.24, 0.245]$) sits exactly at the peak of the modulational band at that height: tracking the band in a at $T = 0.1$, the unstable set is a single interval $\xi \in (0, 0.36)$ at $a = 0.025$ with its maximum 0.00666 at $\xi = 0.242$, and the band edge divided by a tends to the closed-form value $\sqrt{-\alpha_6/\alpha_8} = 11.92$ as $a \to 0$. Second, near T_2 the modulational instability closes at finite amplitude: at $T = 0.06$ the waves are unstable for $a \leq 3 \times 10^{-3}$ and stable at $a = 10^{-2}$, and this is why the certified lower end of segment A rises from 0.060 to 0.0675 at $a = 10^{-2}$. This is consistent with the "nonmonotone, eventually stabilising" regime $0.05 \leq T \leq 0.10$ of [2], although we have not studied that regime systematically.

None of these numbers conflicts with our certified statements, which cover $H \lesssim 0.02$ only.

10. Discussion

10.1. Relation to the Euler problem

Hsiao et al. [3, 4] study the full Euler equations under a sheet with a geometric bending law, with surface tension κ and bending coefficient b, in finite depth h and in infinite depth. Their linear phase speeds $c_n^2 = (1 + \kappa n^2 + bn^4)\tanh(nh)/n$ reduce to our $m_T(n)^2$ for $\kappa = 0$, $h = 1$ and $b = T$, so that the hydroelastic Whitham equation is a model of the $\kappa = 0$ slice of their problem with the same linear dispersion. They resolve the four eigenvalues that bifurcate from the origin in the scaling $\xi = \varepsilon\nu$, obtain a Benjamin–Feir index, and work away from a Wilton-type resonance set (empty for $b \geq 1/14$ or $\kappa \geq 1/2$) and from a characteristic-collision set (finite depth) or a drift degeneracy (infinite depth). Their results and ours are therefore complementary. Their index is the Euler counterpart of our modulational threshold T_0, and we expect the two to differ in value, since the Whitham equation is not the Euler system at the order at which the index is computed. On the other hand, the sideband collision at $\xi \approx 1/2$ and the threshold T_1 do not appear in their analysis, which is local in the Bloch parameter, and neither do statements for all Bloch parameters. Whether the Euler problem has an analogue of T_1 (a range above its modulational threshold in which waves are nevertheless unstable through a collision with the half-wavenumber mode) is a natural question that our results suggest but cannot answer; the linear part of the collision condition ($\Omega(\xi) = \Omega(1+\xi)$ with the same dispersion relation) is the same, but the coupling coefficient that decides the Krein split is not.

The rigorous description of a modulational threshold in finite depth by Berti, Maspero and Ventura [15] is the closest structural analogue of the transition at T_0: a unique critical depth, purely imaginary small eigenvalues on one side, a figure-eight on the other. In the Whitham setting the leading coefficient is explicit (Theorem 3); what is specific to our problem is that, in the certified regions, the modulational threshold is not the stability threshold.

10.2. Limitations

We list what our results do not cover. (i) Amplitude: everything is for $a \leq 10^{-2}$, that is, $H \lesssim 0.02$ in units of the depth, whereas the numerical picture of Section 9 extends to $H = 0.5$. The cost of the band-core certificate grows like $1/a$ at small amplitude but is modest at $a \sim 10^{-2}$, so a moderate extension in amplitude looks feasible; the outer-region certificate is cheap. (ii) Thresholds: near T_0 and T_1 the amplitude windows shrink to zero. Near T_1 on the stable side this is expected, because numerically the instability appears to extend to $T_1 + O(a)$, and near T_0 on both sides the governing indices vanish; the windows $(T_0 - 10^{-6}, T_0 + 1.3 \times 10^{-8})$ and $(T_1, T_1 + 3.9 \times 10^{-6})$ are not covered. (iii) Small rigidity: we do not treat $T < 0.06$, where the modulational index changes sign again (at T_2, T_D and $T_G = 0.00424$, the zero of $2D - R$), the Stokes expansion fails at the 1:2 resonance T_D, and numerics show instabilities away from $\xi = 0$ that we have not classified. (iv) We prove spectral statements only; nonlinear or orbital stability, and instability in the sense of an $L^2(\mathbb{R})$ eigenfunction, are not addressed. (v) The model is the Whitham equation, not the Euler system.

10.3. How the proofs were produced and checked

The analysis, the code and the checkers were produced within one project, with substantial use of AI agents for derivation, coding and review, and no party independent of the project has re-derived the results. The independence that the checks do provide is the following. Every constant was recomputed from scratch in interval arithmetic rather than taken from the derivation; the load-bearing identities (the closed form of α_6 and α_8, the gauge identity and the threshold formulas) were checked in exact arithmetic; the numerical picture was checked against external benchmarks and against the independent computations of [2]; and the finite-amplitude code was audited twice (once by a separate agent working read-only, and once externally with the same audit brief), with every finding and its resolution recorded (Appendix Appendix B). Several errors were found and corrected in this way, among them a reversed disc-overlap test and an invalid weighted-norm inequality; each of them was located and fixed before the final runs, and the results reported here are from the corrected code. We regard an independent re-derivation of at least the band-core certificates as the most useful next step for confidence in these results.

CRediT authorship contribution statement

Lingsen Meng: Conceptualization, Funding acquisition, Formal analysis, Writing – original draft, Writing – review & editing.

Acknowledgements

This work was supported by the National Science Foundation under Grant EAR-2506181.

Declaration of competing interest

The author declares no known competing financial interests or personal relationships that could have appeared to influence the work reported in this paper.

Data availability

The code of all proofs and checkers, the task files, the coverage reports and the numerical scripts are available at Zenodo, `https://doi.org/10.5281/zenodo.22973877`. Raw leaf records of the computer-assisted proofs are archived with their sha256 hashes and are available on request.

Declaration of generative AI and AI-assisted technologies in the manuscript preparation process

During the preparation of this work the author used Claude (Anthropic) in order to draft and revise the text of the manuscript. After using this tool, the author reviewed and edited the content as needed and takes full responsibility for the content of the publication. The use of AI tools in the research itself (derivations, code and audits), and the author's own contributions (key ideas of the solution strategy, the choice of direction and the decisions at the main forks), are described in Appendix Appendix C.

Appendix A. The scaled pencil of the band-core certificate

Fix (T, a, ξ) with $a \neq 0$ and $0 < |\xi| < 1$, and let $A = A(\xi)$, $D = \operatorname{diag}(n+\xi)$, so that $M = DA$ (Section 2). All operators below act on sequences indexed by $n \in \mathbb{Z}$; the certificate works with the truncation $|n| \leq 12$ plus a Schur complement for the tail, and every identity below holds for the infinite operators and for the truncations alike.

Step 1 (the factor ξ). Put $E = \xi D^{-1} = \operatorname{diag}(e_n)$ with $e_0 = 1$ and $e_n = \xi/(n+\xi)$ for $n \neq 0$. Since D is invertible for $\xi \notin \mathbb{Z}$,

$$M\varphi = \xi\nu\varphi \iff DA\varphi = \xi\nu\varphi \iff A\varphi = \nu E\varphi.$$

Thus the eigenvalues $\mu = \xi\nu$ of M correspond to the values of ν at which the pencil $A - \nu E$ has a kernel. A is real symmetric and E is real diagonal, so the pencil is real symmetric.

Step 2 (the translation mode). Let $g_n = n\hat{f}_n$ (the Fourier coefficients of $-if'$). Differentiating the travelling-wave equation gives $A(0)g = 0$: for $n \neq 0$ this is $\mathcal{L}_0 f' = 0$ divided by n, and for $n = 0$ the row reads $-2\sum_m \hat{f}_{-m}\, m\hat{f}_m = 0$, which holds because $\hat{f}$ is even. Since $A(\xi) - A(0) = -\operatorname{diag}(m_T(n+\xi) - m_T(n))$ and $g_0 = 0$,

$$(A - \nu E)g = \xi w, \qquad w_n = -\Big(\delta_n + \frac{\nu}{n+\xi}\Big)g_n, \qquad \delta_n = \frac{m_T(n+\xi) - m_T(n)}{\xi}.$$

Pairing n with $-n$ (note $g_{-n} = -g_n$, so $g_{-n}^2 = g_n^2$) and using $\delta_n + \delta_{-n} = \xi\sigma_n$ with the second divided difference $\sigma_n = (m_T(n+\xi) + m_T(n-\xi) - 2m_T(n))/\xi^2$, and $\frac{1}{n+\xi} + \frac{1}{-n+\xi} = \frac{2\xi}{\xi^2-n^2}$, one obtains

$$g^{\mathsf{T}}(A - \nu E)g = \xi\, g^{\mathsf{T}}w = \xi^2\tau, \qquad \tau = -\sum_{n>0} g_n^2\Big(\sigma_n + \frac{2\nu}{\xi^2 - n^2}\Big).$$

Step 3 (congruence). Let $X = I + (g - e_1)e_1^{\mathsf{T}}$, the identity with its column 1 replaced by g; X is invertible because its $(1,1)$ entry is $g_1 = a/2 \neq 0$ and it differs from I only in that column ($\det X = g_1$ for the truncation). Let Y be the identity with the entry $(1,1)$ replaced by $1/(a\xi)$. Then

$$Q(\nu) = YX^{\mathsf{T}}(A - \nu E)XY$$

has the entries

$$Q_{ij} = (A - \nu E)_{ij}\ (i, j \neq 1), \qquad Q_{i1} = Q_{1i} = \frac{w_i}{a}\ (i \neq 1), \qquad Q_{11} = \frac{\tau}{a^2},$$

because column 1 of $(A-\nu E)X$ is $(A-\nu E)g = \xi w$ and $(X^{\mathsf{T}}(A-\nu E)X)_{11} = g^{\mathsf{T}}(A-\nu E)g$. $Q(\nu) = Q_0 - \nu Q_1$ is real symmetric and affine in ν.

Equivalence. X and Y are invertible for $a \neq 0$, $\xi \neq 0$, so $\ker Q(\nu) = (XY)^{-1}\ker(A-\nu E)$, and for the truncated matrices

$$\det Q(\nu) = \frac{g_1^2}{a^2\xi^2}\det(A-\nu E) = \frac{1}{4\xi^2}\det(A-\nu E).$$

Hence, for $\xi \neq 0$, ν is a zero of the pencil Q if and only if $\xi\nu$ is an eigenvalue of M, with eigenvector $\varphi = XY\psi$; $\psi \in \ell^1$ gives $\varphi \in \ell^2$ because g decays exponentially.

No singularities remain. The entries of Q are bounded and analytic in ξ near 0 and bounded as $a \to 0$. Indeed $g_n = n\hat{f}_n = O(a^{|n|})$ by Lemma 8, so w_i/a and τ/a^2 are bounded uniformly in a (for $n = \pm 1$ one has $g_{\pm 1}/a = \pm 1/2$ exactly, which is how the implementation uses the amplitude: a enters as the Taylor-model value on the box, so the division is exact and not a division by an enclosure containing 0; the certificate is only run for $a \geq a_{\mathrm{lo}} > 0$); δ_n and σ_n are divided differences of the analytic function m_T at $n \neq 0$ and are analytic in ξ; the terms $\nu/(n+\xi)$ and $2\nu/(\xi^2 - n^2)$ occur only for $n \neq 0$; and the entries $(A-\nu E)_{ij}$ with $i, j \neq 1$ are analytic in ξ because E is. In the certificate, δ_n and σ_n are enclosed by their Taylor polynomials in ξ of degree 12 (even terms to degree 10 for σ_n) with Cauchy remainders on the discs $|z-n| = 0.4$, on which m_T is analytic and zero-free for $n \geq 1$ (Section 7.4).

The limits. The statement is for $\xi \neq 0$ and $a \neq 0$. At $\xi = 0$ the three cluster eigenvalues of M are real by continuity: they stay in the certified cluster disc and are real for every $\xi > 0$ in the box. The certificate makes no statement at $a = 0$ and is not needed there.

Appendix B. Reproducibility, data and audit

Appendix B.1. Software and data

All interval computations use Arb [16] through python-flint 0.9.0. The computer-assisted layer works with 192-bit balls directly. The first-layer checkers were written against the interval type of mpmath, whose elementary functions are not proved to round outward; we therefore run them with a drop-in replacement of that type, in which every value is a pair of exact endpoints and every operation (arithmetic, square root, exponential, and the conversion of decimal inputs) is rounded outward by Arb (`arb_port/arbiv.py`, with its own unit tests against 200-digit reference values). In addition, every step of these checkers that previously left the interval type (constants evaluated with round-to-nearest functions, bisection and root-finding for amplitude thresholds, and boxes rebuilt from rounded decimal strings) was rewritten to use Arb enclosures, with each inequality tested as an upper bound against a lower bound, and the amplitude thresholds obtained by bisection or root-finding are reduced by a safety factor and verified again in interval arithmetic. Printed thresholds are rounded down. Each output file records the sha256 of the checker and of the interval backend. Exact identities use sympy. Production runs were array jobs on a university cluster (Python 3.12, one thread per task); the first-layer checkers were rerun under the Arb backend with Python 3.14. No checker relies on `assert` for a certified step. Raw leaf records (several GB compressed) are archived with their sha256 hashes and are available on request; the task files, coverage reports and all checkers are in the repository. The checkers that assemble the theorems, and the first 16 hexadecimal digits of their sha256 on 26 September 2026, are listed in Table B.3.

statement	checker	sha256 (prefix)
Prop. 2	`paper/checks/check_thresholds.py`	`d1221a53cfa610e5`
	`paper/checks/check_2DmR_arb.py`	`a3a039d215f4159e`
Lemma 1	`paper/checks/check_gauge.py`	`d41a614df2b07eb2`
Thm. 4(A)	`mi_instability/check_mi_instability.py`	`c91ffcc9fe232588`
Thm. 4(B)	`sideband_theorem/check_sideband_ext.py`	`acd02cd0dd0e478f`
Thm. I	`stability_theorem/check_outer_stability.py`	`4afd5c92652f0b5f`
Thm. J	`stability_theorem/check_middle_band.py`	`1ecc29ceee4afbc8`
Thm. K	`stability_theorem/check_band_core_arb.py`	`d2827b54de2268be`
Thm. K^+	`stability_theorem/sup_phi.py`	`60fdd363be329bd9`
	`check_band_core_sup.py`	`9927fb29e944b440`
near T_1	`stability_theorem/check_near_T1.py`	`171c9bdd735a86c3`
Thm. 6	`stability_theorem/scaled/check_layer1_s.py`	`42c594113dde971d`
Thm. 5(A,B)	`cap/check_combined.py`	`ff7d28061b48e44a`
Thm. 5(C)	`cap/stable_C/check_C_combined.py`	`0143b5b3a0fc6fd9`
	`cap/stable_C/check_C_bigT.py`	`bf9b77edbdea2890`
	`cap/stable_C/check_C_T10plus.py`	`0ddcf956d72d056b`
	`cap/stable_C/approved_manifests.py`	`e6bab6d8021808b2`
coverage	`cap/stable_C/check_C_coverage.py`	`d005a6d44d6c66e4`
phase diagram	`phase_diagram/check_phase_diagram.py`	`fc67e22046dba7d3`
interval backend	`arb_port/arbiv.py`	`61975ab2a441e83c`
	`arb_port/rig.py`	`56e05d2c53371343`
	`arb_port/check_sweep_kv.py`	`f9348dc6e26072c1`

Table B.3: Assembly checkers. The certificate code of the computer-assisted layer is `cap/cap_core.py` (`d2ea9008`…), `cap/stable_C/cap_stab.py` (`1160c5e0`…) and `cap/stable_C/core_C.py` (`5afd160c`… for $T \leq 0.70$, `64108347`… for $T \geq 0.70$; both versions are archived and re-hashed by the coverage checker).

Appendix B.2. Audit

Before the final runs the finite-amplitude code and the assembly were audited by a separate agent with read-only access, following a written brief, and the same brief and code bundle were sent to an external auditor. The internal audit found no error that would make a stated result false. The findings of the two audits that required action were: an assembly that did not verify all the first-layer ingredients it relied on and did not check the Bloch range of each task; provenance that was not enforced (the sweep records did not carry code hashes, and the coverage check did not bind leaves to the proof code or to the task file); a union bound for two overlapping discs that fails when one disc is nested in the other; a tail-gap bound in Theorem I evaluated at one mode only; an unproved lower bound $|m_T(z)| \geq m_T(\operatorname{Re} z)$ for complex arguments; a symmetry test in the scaled middle band that used the unscaled symbol; and certified radii rounded to nearest instead of downward. All were fixed, every affected computation was rerun with the corrected code, and the assemblies now reject any record whose code hash differs from the archived code. The full list, with the resolution of each item, is in the repository (`AUDIT_2026-09-25.md`). A second audit, prompted by an external review, read every first-layer checker line by line for steps that leave interval arithmetic. It found three places where a certified quantity was not re-verified (an amplitude threshold from bisection, a root returned by a root finder) or was printed rounded to nearest, and a number of constants evaluated in round-to-nearest arithmetic with margins larger than the possible error by at least ten orders of magnitude. All were rewritten as described above and every first-layer result was recomputed. No conclusion changed; the largest change is in the two slabs of Theorem 4(B) closest to T_0, whose amplitude thresholds decreased by $\sim 11\%$ (`arb_port/RIGOR_AUDIT.md`).

Appendix C. Use of AI tools in the research

The research reported here was carried out with extensive use of AI systems, under the direction of the author, and we describe that use here because it bears on how the results should be checked. The author contributed key ideas of the solution strategy, chose the research direction, and made the decisions at the main forks of the project (which questions to pursue, which approaches to adopt or abandon, and which computations to run); the AI systems carried out the derivations, the code and the computations within that frame.

Phases. In a first phase (5–12 September 2026) the problem was posed by the author and worked on in a controller–worker arrangement in which general-purpose language models (OpenAI models accessed through ChatGPT) acted as the main researcher and as an auditor in separate conversations, exchanging results through files and a round protocol. This phase produced the single finite-amplitude certificate at $T = 0.1$ and a transition theorem for the degenerate window at T_0 that is not part of this paper. From 12 September 2026 on, the work was carried out by an AI coding agent (Claude Code, Anthropic) working directly in the project repository, which produced the remaining derivations, all interval-arithmetic code and checkers, the cluster job scripts and the drafts of this manuscript.

What the tools were used for. Symbolic derivations (in each case re-derived as an exact identity by a computer algebra system, not trusted from the model's text); writing the interval-arithmetic proofs and the checkers that assemble them; running the computations on a university cluster; numerical exploration; and searching and summarising the literature (every citation is checked against its source before submission).

How the output was checked. No theorem in this paper rests on text produced by a model: every theorem is backed by a checker that re-computes its constants in interval or exact arithmetic and records the hash of the code that produced it. The main defences against model error were (i) external benchmarks with known answers (the Hur–Johnson threshold, KdV stability, the translation kernel), (ii) independent code paths that do not share modelling assumptions (e.g. exact Schur reduction against direct diagonalisation), (iii) exact arithmetic for identities with cancellations, and (iv) two audits of the finite-amplitude code, one by a separate agent with read-only access and one external with the same brief (Appendix Appendix B). These checks found real errors in model-written code and arguments, among them a reversed inequality in a disc-overlap test, a lower bound applied outside its range, a residual test that shared an indexing error with the solver it checked, and a Schur reduction that dropped off-diagonal coupling and produced a spurious instability; each was corrected before the final runs. We note, however, that these checks are not a substitute for an independent re-derivation by a person outside the project, which has not been done.

References

[1] E. Dinvay, H. Kalisch, D. Moldabayev, E. I. Părău, The Whitham equation for hydroelastic waves, Appl. Ocean Res. 89 (2019) 202–210. doi:10.1016/j.apor.2019.04.026.

[2] M. V. Flamarion, J. Adriazola, Stability of periodic traveling waves for the hydroelastic Whitham equation, Wave Motion 141 (2026) 103675. doi:10.1016/j.wavemoti.2025.103675.

[3] T.-Y. Hsiao, Z. Li, Y. Zhang, C. Zhu, Benjamin–Feir spectrum of hydroelastic Stokes waves, arXiv:2606.09657 (2026).

[4] T.-Y. Hsiao, Z. Li, Y. Zhang, C. Zhu, Modulational spectrum of infinite-depth hydroelastic Stokes waves, arXiv:2608.04938 (2026).

[5] V. M. Hur, M. A. Johnson, Modulational instability in the Whitham equation for water waves, Stud. Appl. Math. 134 (2015) 120–143. doi:10.1111/sapm.12061.

[6] V. M. Hur, M. A. Johnson, Modulational instability in the Whitham equation with surface tension and vorticity, Nonlinear Anal. 129 (2015) 104–118. doi:10.1016/j.na.2015.08.019.

[7] M. Cadiot, Constructive proofs of existence and stability of solitary waves in the Whitham and capillary-gravity Whitham equations, Nonlinearity 38 (2025) 035021. doi:10.1088/1361-6544/adb5e8.

[8] R. Castelli, J.-P. Lessard, Rigorous numerics in Floquet theory: computing stable and unstable bundles of periodic orbits, SIAM J. Appl. Dyn. Syst. 12 (2013) 204–245. doi:10.1137/120873960.

[9] G. Arioli, H. Koch, Spectral stability for the wave equation with periodic forcing, J. Differential Equations 265 (2018) 2470–2501. doi:10.1016/j.jde.2018.04.040.

[10] K. E. M. Church, J.-P. Lessard, Rigorous verification of Hopf bifurcations in functional differential equations of mixed type, Physica D 429 (2022) 133072. doi:10.1016/j.physd.2021.133072.

[11] N. Sanford, K. Kodama, J. D. Carter, H. Kalisch, Stability of traveling wave solutions to the Whitham equation, Phys. Lett. A 378 (30–31) (2014) 2100–2107. doi:10.1016/j.physleta.2014.04.067.

[12] B. Deconinck, J. N. Kutz, Computing spectra of linear operators using the Floquet–Fourier–Hill method, J. Comput. Phys. 219 (2006) 296–321. doi:10.1016/j.jcp.2006.03.020.

[13] J. D. Carter, M. Rozman, Stability of periodic, traveling-wave solutions to the capillary Whitham equation, Fluids 4 (2019) 58. doi:10.3390/fluids4010058.

[14] R. Creedon, B. Deconinck, O. Trichtchenko, High-frequency instabilities of a Boussinesq–Whitham system: a perturbative approach, Fluids 6 (2021) 136. doi:10.3390/fluids6040136.

[15] M. Berti, A. Maspero, P. Ventura, Benjamin–Feir instability of Stokes waves in finite depth, Arch. Ration. Mech. Anal. 247 (2023) 91. doi:10.1007/s00205-023-01916-2.

[16] F. Johansson, Arb: efficient arbitrary-precision midpoint-radius interval arithmetic, IEEE Transactions on Computers 66 (8) (2017) 1281–1292. doi:10.1109/TC.2017.2690633.